

Chapter 3

Multiple Model Resonant Control

In this chapter, a new control method, able to attenuate the multi-mode vibration of a flexible structure with varying natural frequencies, is presented. The method is referred to as multi-model multi-mode resonant control (M⁴RC). Two M⁴RC design cases are discussed. In the first case, the M⁴RC design assumes that all of the possible variations to the plant natural frequencies are *a priori known*. In the second case, this assumption is relaxed. Only the upper and lower bounds of the operating region are presumed to be *a priori known*. This chapter starts with a brief introduction to resonant control. The resonant controller structure and its characteristics are presented in Section 3.2. In Section 3.3, discrete-time resonant control is derived using a bilinear transformation, and the stability of the discrete-time resonant control system is proven using the passivity theorem. The multiple model control approach that forms the basis of the proposed control method is presented in Section 3.4. The proposed multiple model resonant control method is then presented in Section 3.5. An evaluation of the proposed control method through simulation studies is given in Section 3.6. The experimental results used to verify the simulation results are reported in Section 3.7.

3.1 Introduction

As shown in Chapter 2, one of the characteristics of flexible structures is their highly resonant nature. For the case of the cantilever beam used in this research this characteristic is made evident by the relatively large vibration at or near to the natural frequencies of the structure, as shown in Fig. 3.1. From the

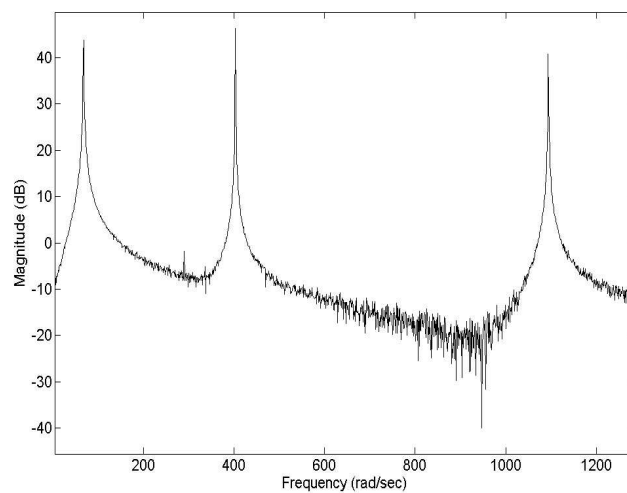


Figure 3.1. Frequency response of a flexible cantilever beam.

figure, it is clear that suppressing the vibration of a structure at or very close to the natural frequencies of the structure is more important than suppressing the vibration at other frequencies. However, suppressing the vibration at one or more natural frequencies may excite or amplify other natural frequencies. Therefore, one important design requirement for flexible structure control is to achieve high attenuation for modes of interest without driving the other modes into instability or exciting and amplifying the vibration of other modes.

As stated in Chapter 1, a resonant controller has necessary characteristics that satisfy the design requirements for multi-mode vibration attenuation of flexible structures investigated in this research. Exploiting the highly resonant charac-

teristic of the flexible structure, the resonant controller only applies high gain at or close to the natural frequencies of interest, and is therefore able to suppress the vibration at those frequencies without causing adverse effects at other frequencies. In the following section, a further analysis on the characteristics of a resonant controller is presented.

3.2 Structure of a Resonant Controller

Consider a flexible structure with a collocated piezoelectric sensor-actuator pair attached to it as shown in Fig. 3.2 [114]. The piezoelectric patch at the top of the beam is used as an actuator, while the patch on the bottom serves as a sensor. The controller output is $u(t)$, the sensor voltage is $y(t)$, and the external disturbance is $f(t)$. The block diagram for the control system can be depicted as in Fig. 3.3. The approximate transfer function of the flexible structure is the truncated version of (2.47):

$$G_M(s, x) = \sum_{m=1}^M \frac{y_m(x)y_m(x_1)}{s^2 + 2\zeta_m\omega_m s + \omega_m^2} \quad m = 0, 1, 2, \dots, M \quad (3.1)$$

where M is the highest resonant mode to be controlled.

The resonant controller $K(s)$ as given in [113, 114] is described by

$$K(s) = \sum_{m=0}^M K_m(s) \quad (3.2)$$

with

$$K_m(s) = k_{cm} \frac{s^2 + 2\zeta_{cm}\omega_m s}{s^2 + 2\zeta_{cm}\omega_m s + \omega_m^2} \quad (3.3)$$

where ω_m is the m^{th} controller centre frequency, which is the same as the m^{th} natural frequency of the vibrating system, ζ_{cm} is the m^{th} mode controller damping factor, and k_{cm} is the gain for the m^{th} mode controller.

The controller $K_m(s)$ is a second-order filter with two zeros and two poles. One zero is at the origin and the other is a real zero in the Left Half Plane

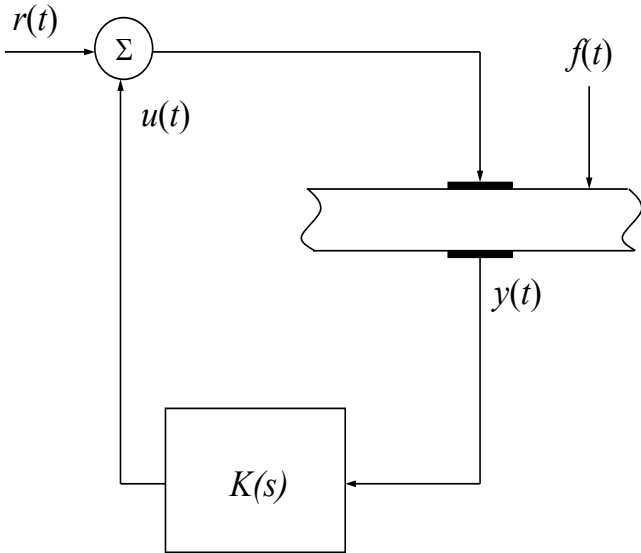


Figure 3.2. Flexible structure control system.

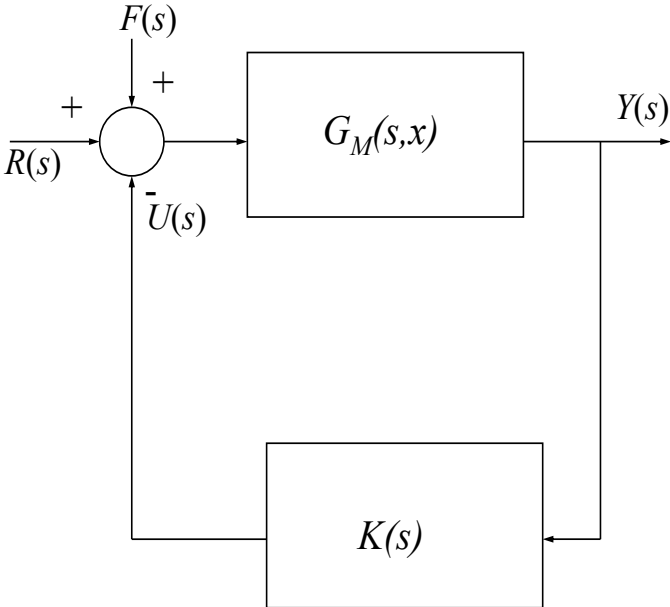


Figure 3.3. Block diagram of resonant control.

(LHP) of the s -plane. The controller has a band-pass filter which has a high Q characteristic, with a high gain at the natural frequency of the system and a sharp drop in gain away from the natural frequency of the system. This highly resonant characteristic of the controller is shown in Fig 3.4. The transfer function

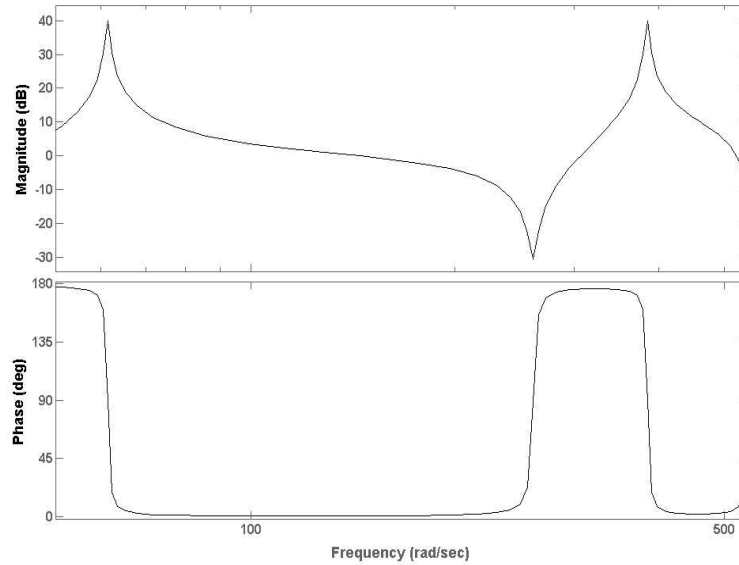


Figure 3.4. Frequency response of a dual mode resonant controller.

of the closed loop system is

$$\frac{Y(s)}{R(s)} = \frac{G_M(s)}{1 + G_M(s)K(s)}. \quad (3.4)$$

To suppress vibration the term on the right hand side of (3.4) must be small. Hence it can be seen that the feedback is effective only for the frequency range close to the natural frequency of the system where $|G_M(j\omega)K(j\omega)|$ is large. This characteristic makes the controller robust to spillover effects caused by mode truncation, because the controller will not excite the unmodeled dynamics away from the frequency of concern. The effect of the controller is localized to each mode of a structure. Due to this localized effect of the controller, a single sensor-actuator pair can be used to suppress multi-mode vibration in the structure.

Equation (3.2) shows that to control M modes of vibration, M controllers can be arranged in parallel to form a summation of the different mode controllers. Each of the mode controller parameters, ω_m , ζ_{cm} , and k_{cm} in (3.3) is designed independently, and solely based on the plant parameters for the corresponding mode. The parameter k_{cm} in (3.3) can be set to zero for a particular m if that mode is not to be controlled, giving designers the freedom to choose which mode they wish to control.

Of all the three controller design parameters, only the controller centre frequency is sensitive to variations of the plant parameters. To achieve optimum attenuation, the controller centre frequency must be set to be the same as the natural frequency of the plant. In contrast, the controller damping ratio, ζ_{cm} , and the controller gain, k_{cm} , are not sensitive to variations of the plant parameters, and there is no simple relationship between ζ_{cm} and k_{cm} with the plant parameters. Optimum values of ζ_{cm} and k_{cm} can be found through a trial and error procedure. The parameters ζ_{cm} and k_{cm} have differing effects on control performance. As the chosen value of ζ_{cm} is decreased, the attenuation at the corresponding natural frequency becomes higher. If, however, the selected value of ζ_{cm} is too small, the vibration at the other frequencies outside this natural frequency will be amplified. The effect of k_{cm} selection demonstrates a converse result to that of the ζ_{cm} selection. The higher the value of k_{cm} , the higher the attenuation associated with that natural frequency. However, if the selected value of k_{cm} is too high, then the vibration amplitudes for the other frequencies outside this natural frequency will be amplified. The sensitivity of the controller parameters to variations of the plant parameters, which affect the control system performance, is demonstrated in the following example.

Example 3.2.1

A resonant controller $K(s)$ with $k_{cm} = 10$, $\zeta_{cm} = 0.01$, and $\omega = 62.8$ rad/sec is used to control a second-order plant in five different cases. In the first case the controller is used to control the nominal plant, $G_1(s)$. In the second and third cases, the natural frequency of $G_1(s)$ is decreased and increased by 5% to form $G_2(s)$ and $G_3(s)$, respectively. In the fourth and fifth cases the damping factor of the plant are two times larger and ten times lower, respectively, compared to the damping factor of $G_1(s)$. This yields $G_4(s)$ and $G_5(s)$. The parameters and the transfer function of the plant for all five cases are shown in Table 3.1.

Case	ζ	ω (rad/sec)	Transfer function
1	0.001	62.8	$G_1(s) = \frac{1}{s^2+0.126s+3947.8}$
2	0.001	59.7	$G_2(s) = \frac{1}{s^2+0.1196s+3562.9}$
3	0.001	65.9	$G_3(s) = \frac{1}{s^2+0.1326s+4352.5}$
4	0.002	62.8	$G_4(s) = \frac{1}{s^2+0.251s+3947.8}$
5	0.0001	62.8	$G_5(s) = \frac{1}{s^2+0.0126s+3947.8}$

Table 3.1. Models' parameters used in the example.

The responses of the controlled system for all the cases are shown in Fig. 3.5 and Fig. 3.6. Fig. 3.5 shows that a significant degradation of the attenuation performance occurs for a small change in the natural frequency of the plant. The attenuation performance decreases around 13 dB for only a 5% change in the plant natural frequency. However, the attenuation performance is not sensitive to the plant damping factor variation. The attenuation performance only varies around 1 dB for 2 times (100%) and 10 times variations in the plant damping factor as shown in Fig. 3.6.

In the implementation of the resonant controller, it is assumed that the natural frequencies of the structure are known through a modeling process or modal

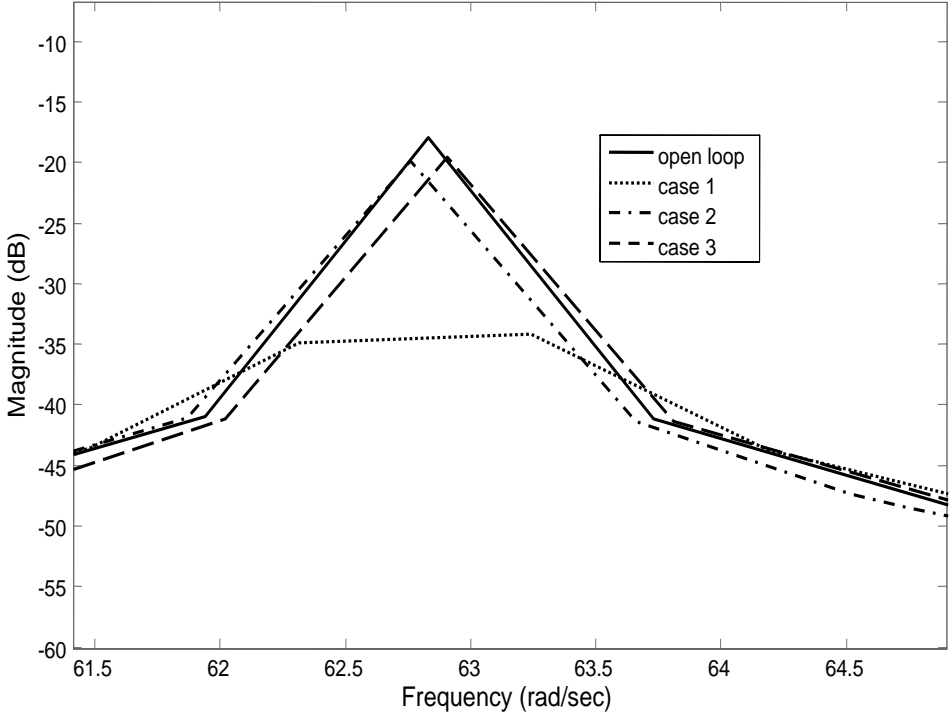


Figure 3.5: Closed-loop responses for variations in a plant natural frequencies.

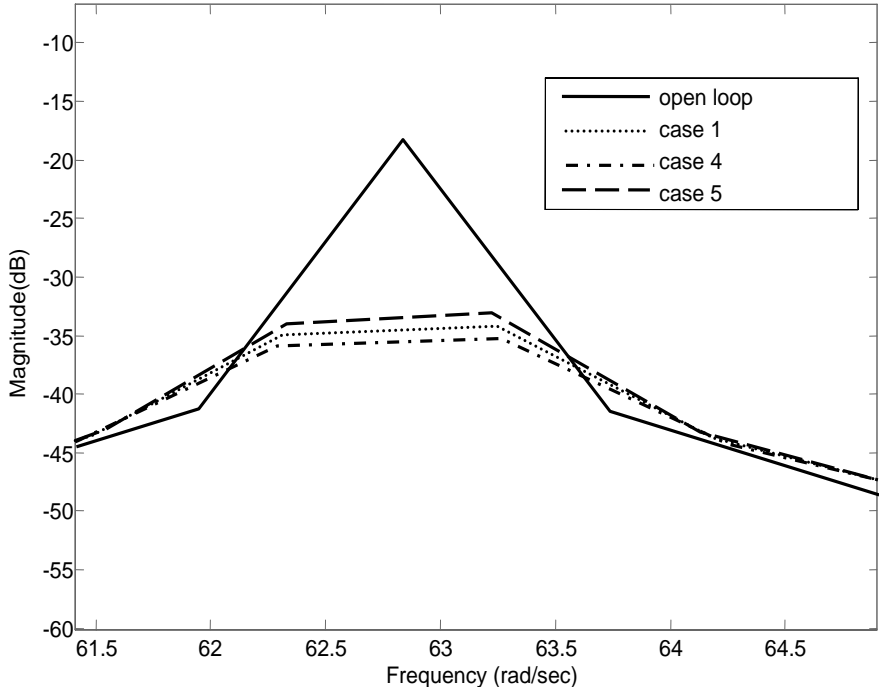


Figure 3.6: Closed-loop responses for variations in a plant damping factors.

testing measurement. Then, based only on the natural frequencies of the structure, the resonant controller can be designed. This promotes a simple design procedure suitable for a real-time implementation. However, since a resonant controller is designed for specific narrow frequencies and is very sensitive to the structure natural frequencies variations, then it becomes ineffective if the structure natural frequencies are altered due to changes in its configuration and or loading.

3.3 Discrete-time Resonant Control

To embed the resonant control algorithm in a real-time micro controller platform, the continuous resonant controller (3.2) must be transformed into its corresponding discrete-time form. There are five common methods that can be used to discretize continuous systems into discrete-time systems: the impulse-invariant method, the backward-difference method, the forward-difference method, the bilinear transformation method, and the step-invariance method [107].

In this research, the selection of the discretization method is based on preservation of the passivity of the continuous systems through the discretization process and practical minimisation of the computational load of the discretization method. A method that preserves the passivity characteristic of continuous resonant control is chosen to ensure stability. A proof for this is given in Section 3.3.1 and 3.3.2.

Not all of the five methods mentioned above preserve the passivity of the continuous systems. Jiang [58] examined the passivity preservation properties of the five methods. The conclusion of the study is that only backward-difference, bilinear transformation and impulse-invariant methods are capable of preserving the passivity of the continuous system. Furthermore, of these three methods, the bilinear transformation method has the lowest computational demand [107].

Therefore, the bilinear transformation is chosen in this research as the discretization method.

Applying the bilinear transformation

$$s = 2f_s \frac{z-1}{z+1} \quad (3.5)$$

to (3.3), where f_s is the sampling frequency, one obtains the discrete-time resonant controller for the m^{th} mode as

$$K_m(z) = k_{dm} \frac{A_m z^2 + B_m z + C_m}{z^2 + D_m z + E_m} \quad (3.6)$$

with

$$A_m = \frac{4f_s^2 + 4f_s \zeta_{cm} \omega_m}{4f_s^2 + 4f_s \zeta_{cm} \omega_m + \omega_m^2}, \quad (3.7)$$

$$B_m = \frac{-8f_s^2}{4f_s^2 + 4f_s \zeta_{cm} \omega_m + \omega_m^2}, \quad (3.8)$$

$$C_m = \frac{4f_s^2 - 4f_s \zeta_{cm} \omega_m}{4f_s^2 + 4f_s \zeta_{cm} \omega_m + \omega_m^2}, \quad (3.9)$$

$$D_m = \frac{2\omega_m^2 - 8f_s^2}{4f_s^2 + 4f_s \zeta_{cm} \omega_m + \omega_m^2}, \quad (3.10)$$

$$E_m = \frac{4f_s^2 - 4f_s \zeta_{cm} \omega_m + \omega_m^2}{4f_s^2 + 4f_s \zeta_{cm} \omega_m + \omega_m^2}, \quad (3.11)$$

and k_{dm} is the gain for the m^{th} controller. From (3.6), the discrete-time resonant control law $u(k)$ for sampling time k is given by

$$u(k) = \sum_{m=1}^M u_m(k) k_{dm}, \quad (3.12)$$

with

$$u_m(k) = A_m y(k) + B_m y(k-1) + C_m y(k-2) - D_m u_m(k-1) - E_m u_m(k-2) \quad (3.13)$$

where $y(k)$ is the controlled output at sampling time k .

The continuous resonant control system is proven to be stable [114]. In the next two sections there is a discussion on system stability and a proof that for a discrete-time resonant control system preservation of a system passivity using bilinear transformation also preserves the stability of the system.

3.3.1 Input-output Stability

One general approach that is widely used to address the stability problems that arise in control systems is the input-output stability theory [56, 99]. This stability theory considers the effect of external inputs on a system's stability. If a system is described by an operator W that maps an input space \mathcal{U} to an output space \mathcal{Y} , the concept of the input-output stability is based on the properties of \mathcal{U} and \mathcal{Y} . If a property L_p space of the input is invariant under the transformation W , the system is said to be L_p -stable [99]. For any fixed $p \in [1, \infty)$, variable u is said to belong to L_p if the L_p norm of u exists [56] or

$$\|u\|_p \triangleq \left(\int_0^{\infty} |u(t)|^p dt \right)^{1/p} < \infty, \quad (3.14)$$

and for $p = \infty$

$$\|u\|_{\infty} \triangleq \sup_{t \geq 0} |u(t)| < \infty. \quad (3.15)$$

Then the system represented by the operator W is said to be L_p -stable if $u \in L_p$ is mapped into $y \in L_p$. When $p = \infty$, L_p -stability is also referred to as bounded-input bounded-output (BIBO) stability. The familiar BIBO stability notion contends that if the input signal is finite, then the output signal also must be finite.

Consider now a canonical feedback system as shown in Fig. 3.7. G_1 and G_2 are operators that act on input u_1 and u_2 , respectively, to produce output y_1 and y_2 . r is an external input to the system. The equations describing the system are given by

$$\begin{aligned} y_1 &= G_1 u_1 \\ y_2 &= G_2 u_2 \end{aligned} \quad (3.16)$$

The stability problem then is to determine conditions for G_1 and G_2 , so that if u_1 and u_2 are in the same class L_p , then y_1 and y_2 are in the same class.

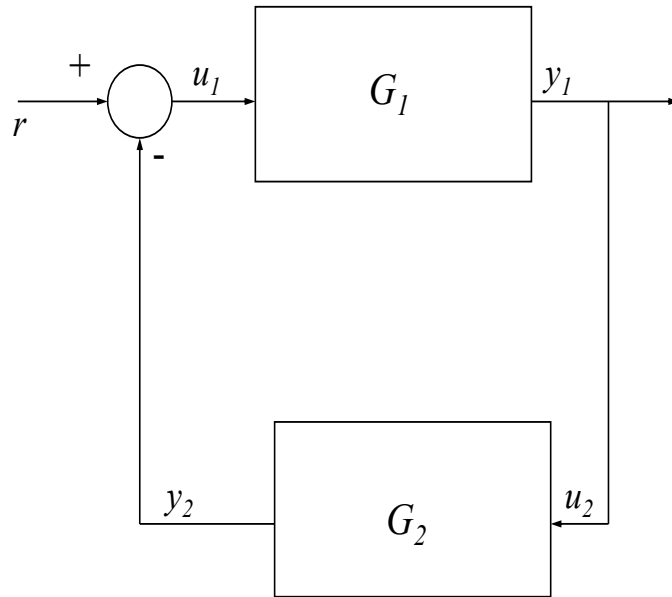


Figure 3.7. A canonical feedback system.

One concept, which is widely used in input-output stability problems, is that of passivity [99]. In the passivity concept, a system is considered as a device which interacts with its environment by transforming inputs into outputs. From an energy viewpoint, a passive system can be defined as a system which cannot store more energy than is supplied by some source, with the difference between stored energy and supplied energy, being the dissipated energy [82]. Hence for a bounded input, a passive system will produce bounded output. Therefore it is clear that a passive system is stable in the input-output stability sense.

A fundamental property of passive systems is that the negative feedback interconnection of two passive systems yields a passive system. This property is formalized in the passivity theorem which states that a negative feedback interconnection of two passive system is stable [29]. Therefore, the stability of the feedback system in Fig 3.7 can be achieved by proving that G_1 and G_2 are passive. Another property of passive systems is that a system resulting from the parallel interconnection of passive systems is passive [70].

3.3.2 Stability of a Discrete-time Resonant Control System

As shown in Fig. 3.3, a resonant control system is a feedback interconnection between the truncated plant G_M and the resonant controller K . The stability of the discrete-time resonant control system will be proven using the passivity theorem. To accomplish this, it is sufficient to prove that both the discrete-time controller $K(z)$ and the discretization of truncated plant (3.1) are passive. Furthermore, due to the passivity of the parallel interconnection of passive systems, it is sufficient to prove that the discrete-time controller (3.6) is passive.

Two steps are undertaken in the stability proof. Step 1 proves that the discrete-time controller (3.6) is passive, and Step 2 proves that the discretized truncated plant (3.1) is also passive.

Step 1

In Appendix B, it is stated that a discrete-time system is passive if all the poles of the system lie inside the unit circle and the real value of the system for $z = 1$ is greater than or equal to zero. Therefore it can be proven that the discrete-time resonant controller (3.6) is passive by confirming that all the zeros of (3.6) lie inside the unit circle and that the real value of (3.6) for $z = 1$ is greater than or equal to zero. Write (3.6) as

$$K_m(z) = \frac{P(z)}{Q(z)} = k_{dm} \frac{A_m z^2 + B_m z + C_m}{z^2 + D_m z + E_m}. \quad (3.17)$$

According to the Jury criterion [107] all the poles of (3.17) are inside the unit circle if

1. $E_m < 1$,
2. $Q(z)|_{z=1} > 0$, and
3. $Q(z)|_{z=-1} > 0$.

From (3.11) it can be seen that the first condition is satisfied. Substituting $z = 1$ and $z = -1$, respectively, into $Q(z)$ in (3.17) results in

$$Q(1) = \frac{4\omega_m^2}{4f_s^2 + 4f_s\zeta_{cm}\omega_m + \omega_m^2} > 0 \quad (3.18)$$

and

$$Q(-1) = \frac{16f_s^2}{4f_s^2 + 4f_s\zeta_{cm}\omega_m + \omega_m^2} > 0, \quad (3.19)$$

respectively, which shows that the second and third conditions are also satisfied.

Thus all the poles of $K_m(z)$ lie inside the unit circle. Inserting $z = 1$ in (3.17) results in

$$\operatorname{Re}[K_m(z)] = 0. \quad \forall z = 1 \quad (3.20)$$

Therefore, (3.17) satisfies the conditions for passive systems as in Definition B.2 of Appendix B, and hence the controller (3.6) is passive.

Step 2

Applying the bilinear transformation (3.5) to (3.1) one obtains the transfer function of the discrete-time plant as

$$G(z, x) = \frac{R(z)}{S(z)} = \sum_{m=1}^M \frac{y_m(x)y_m(x_1)(z^2 + 2z + 1)}{a_m z^2 + b_m z + c_m} \quad (3.21)$$

with

$$a_m = 4f_s^2 + 4f_s\zeta_m\omega_m + \omega_m^2, \quad (3.22)$$

$$b_m = -8f_s^2 + 2\omega_m^2, \quad (3.23)$$

and

$$c_m = 4f_s^2 - 4f_s\zeta_m\omega_m + \omega_m^2. \quad (3.24)$$

From (3.21) to (3.24), it can be seen that

$$a_m > c_m, \quad (3.25)$$

$$S(z)|_{z=1} = 4\omega_m^2 > 0, \quad (3.26)$$

and

$$S(z)|_{z=-1} = 16f_s^2 > 0. \quad (3.27)$$

Hence all the poles of (3.21) lie inside the unit circle. Furthermore, by substituting $z = 1$ in (3.21) and because eigenfunctions, $y_m(x)$ and $y_m(x_1)$, have the same sign for collocated systems, then

$$\text{Re}[G(z, x)] = \frac{4y_m^2(x)}{4\omega_m^2} > 0, \quad \forall z = 1. \quad (3.28)$$

Following Definition B.3 of Appendix B, the discrete plant (3.21) is strictly passive.

Hence, the closed loop system comprising the discrete-time resonant controller (3.6) and the plant (3.1) is stable according to passivity theorem.

The control system is stable with respect to incorrect resonant frequencies. The incorrectly specified natural frequencies of the model will only make the controller perform sub optimally without destabilizing the closed-loop system. To obtain optimum performance for a system with varying natural frequencies, a resonant controller based on the multiple model control approach, referred to as M⁴RC, is proposed. Prior to the discussion of the M⁴RC design, a brief review of the multiple model control method is presented in the next section.

3.4 Multiple Model Control

As mentioned in Chapter 1, the multiple model control (MMC) method is a control method that is designed to cope with systems that have varying parameters. MMC is a model-based control method which integrates a bank of model-controller pairs to handle all possible operating conditions. Two approaches to MMC can be found in the literature: the weighting function scheme [5, 22, 40, 48, 119] and the supervisor scheme [6, 38, 100, 75].

Weighting Function Scheme

In the weighting function scheme approach, as shown in Fig. 3.8, a model bank is designed based on *a priori* knowledge of the plant. Corresponding to each model in the bank, a controller is designed. At each step, the output of the plant, y , is compared with the output of the models $y_i, i = 1$ to L . The differences generated from the comparisons are the errors $e_i, i = 1$ to L . Using these errors, a weighting function is used recursively to measure the probability of each model in the model bank representing the current plant. Based on the measurement, suitable weights are given to individual controllers in the controller bank such that the most probable model carries the highest weight. The sum of the weighted controllers' outputs is then used as the control signal to the plant. In this way, control signals from the controllers, $u_i, i = 1$ to L , for models which closely represent the current plant will exert greater influence on the final control signal u .

The most common method used in the weighting function design employs a probability estimate based on Bayes' rule [22, 40, 48]. Using this method, the likelihood of the i^{th} model fitting the plant can be measured, and the weighting value for each corresponding controller can be determined. At the k^{th} step, the probability for the i^{th} model being the true model of the plant is computed as [22]

$$p_{i,k} = \frac{\exp(-\frac{1}{2}e_{i,k}^T C_f e_{i,k}) p_{i,k-1}}{\sum_{j=1}^L \exp(-\frac{1}{2}e_{j,k}^T C_f e_{j,k}) p_{j,k-1}}, \quad (3.29)$$

where

$$e_{i,k} = y_k - y_{i,k}, \quad i = 1 \dots L, \quad (3.30)$$

is the error at the k^{th} step. L denotes the total number of models in the model bank and C_f is the convergence factor used to tune the rate of convergence of the probabilities. The recursion is initialized by assigning equal probability $\frac{1}{L}$ to all models in the bank. At each iteration the new probability, $p_{i,k}$, is calcu-

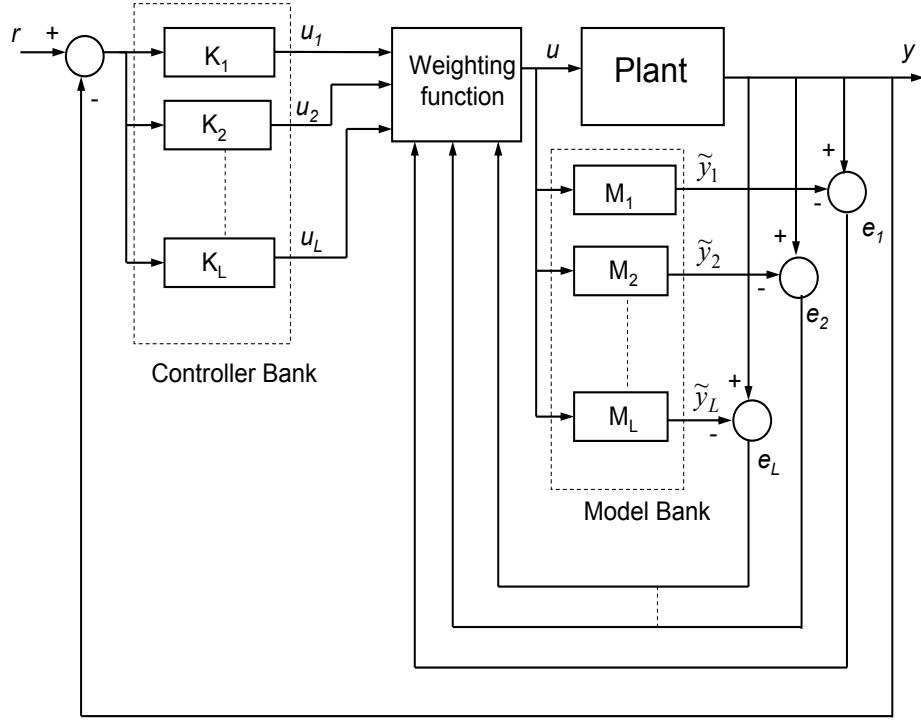


Figure 3.8: Multiple model control method using weighting function scheme.

lated, improving upon the probability calculated at the previous iteration, $p_{i,k-1}$. Equation (3.29) shows that once a probability reaches zero it will remain zero thereafter. A threshold δ is added to prevent $p_{i,k}$ from becoming zero,

$$\begin{aligned} p_{i,k} &= p_{i,k} & \forall p_{i,k} > \delta, \\ p_{i,k} &= \delta & \forall p_{i,k} \leq \delta. \end{aligned} \quad (3.31)$$

At the k^{th} step, a weight $W_{i,k}$ for the i^{th} model is calculated as [130]

$$\begin{aligned} W_{i,k} &= \frac{p_{i,k}}{\sum_{j=1}^L p_{j,k}} & \forall p_{i,k} > \delta, \\ W_{i,k} &= 0 & \forall p_{i,k} = \delta. \end{aligned} \quad (3.32)$$

Then the final control signal applied to the plant is

$$u_k = \sum_{j=1}^L W_{j,k} u_{j,k}. \quad (3.33)$$

From (3.33), it can be seen that the unique feature of this approach is the capability of the weighting function to find a proper combination of control signals

from the individual controllers which can be applied to the plant as the final control signal. Due to the highly resonant characteristic, the resonant controller works effectively only for a narrow-band frequency. For a certain plant, only a controller with a centre frequency that matches or is close to the plant natural frequency will produce an optimum control signal. A weighted combination of several controllers with different centre frequencies will not produce the optimum control signal. For that reason, a multi-model control with a weighting function scheme will not improve the performance of resonant control when the natural frequencies of the system under control are varied. Hence, this multiple-model control method is not suitable for use as a basis for a multi-model controller based on resonant control.

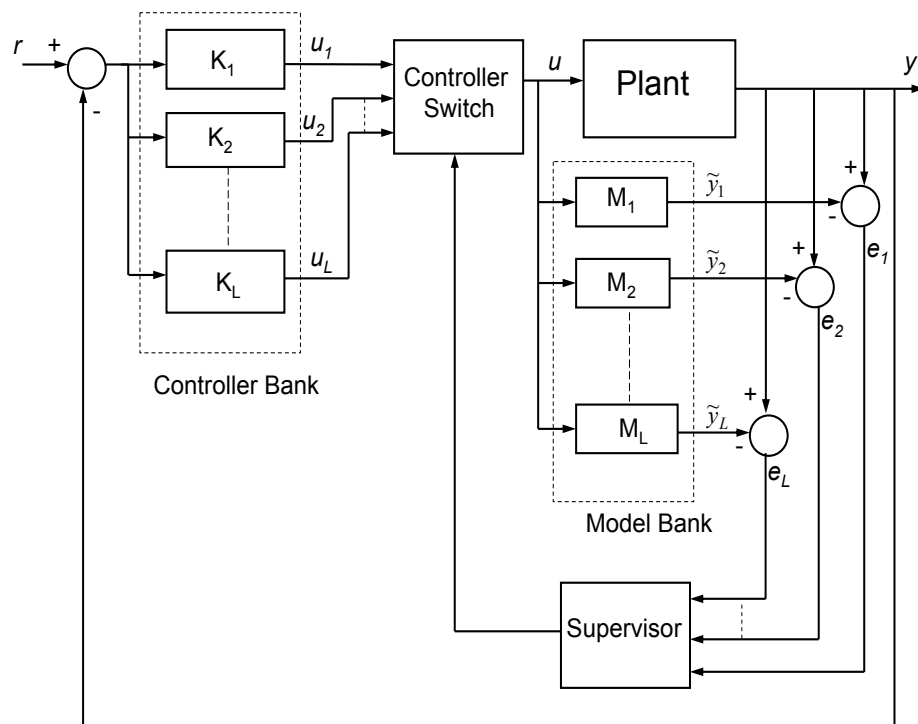


Figure 3.9. Multiple model control method using supervisor scheme.

Supervisor Scheme

In the supervisor scheme approach, as shown in Fig. 3.9, a bank of models and a supervisor scheme are used to choose a model that gives the best approximation

to the current plant condition. A controller corresponding to the model is then used to supply the control action to the plant. In contrast to the weighting function scheme, in the supervisor scheme only a single controller is chosen for the final control action through a switching process in the controller bank. Since only one controller is selected at any instant, then horizon-based error tracking such as minimum mean-squares error (MMSE) is commonly used to design the supervisor [6, 38, 75, 101]. This method identifies which model produces the lowest error over a fixed period of time and selects the corresponding controller as the most suitable for the given condition.

The algorithm for the supervisor scheme can be written as [101]

$$J_l(t) = \alpha e_l^2(t) + \beta \int_0^t e^{-\lambda(t-\tau)} e_l^2(\tau) d\tau, \quad \alpha \geq 0, \beta, \lambda > 0 \quad (3.34)$$

for a continuous-time system or

$$J_l(k) = \alpha e_l^2(k) + \beta \sum_{j=0}^k e^{-\lambda(k-j)} e_l^2(j) \quad (3.35)$$

for a discrete-time system. The error e_l is the difference between the output of the plant, y , and the output of the model L , \tilde{y}_l , as shown in Fig. 3.9. The constants α and β are the weighting factors which are used to weight the importance of current and past errors, respectively. For $\beta = 0$ the index performance (3.34) can be written as

$$J_l(t) \triangleq e_l^2(t). \quad (3.36)$$

The index performance (3.36) is based only on the current errors. It will quickly detect transient peaks in $e_l^2(t)$ resulting in very rapid switching. However, very rapid switching between the controllers may lead to poor system performance [100]. If the current errors weighting factor, α , is set to be zero, the index performance (3.34) becomes

$$J_l(t) \triangleq \int_0^t e^{-\lambda(t-\tau)} e_l^2(\tau) d\tau. \quad (3.37)$$

In the index performance (3.37), the constant λ plays an important role in determining the response of the system. The selection of an appropriate value for λ for a given problem is essentially heuristic and can be different for each model [6]. It is affected by several factors such as the parameter variation period, disturbance effect, and noise effect [65]. For a system with slow parameter variations, small λ should be selected. For a small λ , the index performance (3.37) will approach

$$J_l(t) \triangleq \int_0^t e_l^2(\tau) d\tau, \quad (3.38)$$

and this index is a good indicator of steady-state identifier accuracy which leads the system to select the best model in the model bank. On the other hand, for a system with frequent parameter variations a large value of λ might be chosen. A large value of λ will give more weight to the latest errors resulting in a quick response to abrupt parameter changes. However, disturbance and noise affect the error signal e_l , and a large value of λ makes the index performance very sensitive to noise and disturbance, leading to unwanted switching resulting in poor performance. Hence, for a noisy system and/or a system subjected to disturbance, a small value of λ needs to be chosen.

From the discussion above it can be seen that the choice of λ for a noisy system with frequent parameter variations that are subject to disturbance is conflicting. In such a situation choosing a different set of parameters (i.e., α , β , and λ) can be a difficult task, hence greater knowledge about the system is required. Besides the difficulty of selecting parameters, as can be seen from the second term of (3.34) or (3.35) the switching scheme poses a high computational demand that increases significantly with the number of models employed. Index performance is calculated for each model, and then a comparison is made to determine the minimum index performance. For example, if 100 samples (i.e., $k = 100$ in (3.35)) are required to calculate the performance index for each model, then a further 100 samples are required for every additional model. The computation demand

can be reduced by setting $\beta = 0$, as shown in (3.36). However, as discussed above extremely rapid switching between controllers may occur, resulting in ineffective control. To reduce the computational demand and to avoid too rapid switching, a simple supervisor scheme for use with the M⁴RC method is proposed in the next section.

3.5 Multi-model Multi-mode Resonant Control (M⁴RC)

As discussed in Section 3.2, due to its highly resonant characteristic, resonant control will only give optimum performance when the controller centre frequency coincides with the natural frequency of the system. For a system with varying natural frequencies, even though the system is stable, the closed loop system will not achieve optimum performance. In order to cope with the system natural frequency variations, M⁴RC is proposed.

The M⁴RC design is based on the multiple model control with supervisor scheme. Two design cases are presented. In the first case, *a priori* information about all the plant condition is assumed to be available. From that information, a model bank and its associated controller bank can be designed. In the second case, only the upper and lower bounds of the operating region are *a priori* known.

3.5.1 Case 1: All the Possible Loading Condition are *a priori* Known

Two design problems need to be addressed in the design process for the multiple model control method with supervisor scheme: (i) the design of the supervisor scheme and (ii) the determination of how many models in the model bank are required to span the operating region. Due to the assumption that all of the possible loading conditions are *a priori* known, the second problem is not an

issue. The number of required models is determined from the *a priori* information regarding how many different loading conditions exist in the operating region. This leaves the design of the supervisor scheme as the main focus of the M⁴RC design.

M⁴RC Design

In principle, the role of the supervisor in the multi-model control method is to determine which model in the model bank most closely represents the current plant condition. In the M⁴RC, the models are designed to represent the natural frequencies of the different plant conditions. Since the effectiveness of the resonant control depends on how close the controller centre frequency is to the excitation frequency, a simple supervisor can be designed to replace the MMSE scheme described in (3.35).

From the linearity principle, a linear structure will vibrate with the same frequency as the frequency of excitation signal. Thus the excitation frequency applied to a linear structure can be measured by measuring the output frequency. Using this principle, the determination of the closest model to the current plant can be determined by comparing the plant's output vibration frequency with the centre frequencies of the models. To achieve this for single-mode control, the model bank Model 1 to Model L used in Fig. 3.9 is replaced by the filter bank system shown in Fig. 3.10.

In this approach, a bank of band-pass filters, BPF_{m1} to BPF_{mL} , is used to represent the m^{th} natural frequency of Model 1 to Model L . The representation is achieved by employing a narrow band-pass filter where the centre frequency is the same as the natural frequency of the corresponding model. In this way if the plant vibration signal is injected into the filter bank, the BPF with the closest centre frequency to the vibration signal frequency will produce the maximum output. To identify which model (BPF) gives the maximum output, a decision making

component, formed from an absolute (abs) block, a low-pass filter (LPF), and a maximum (MAX) block, is used. The abs block obtains the absolute value of the vibration signal. The absolute value of the signal is then passed through a LPF to obtain the dc value of the signal. The MAX block is then used to select which LPF produces the maximum dc value. In this way the most appropriate known model and its corresponding controller for the current single-mode frequency can be identified. An output of the filter bank system then sets a switch to select the appropriate plant controller.

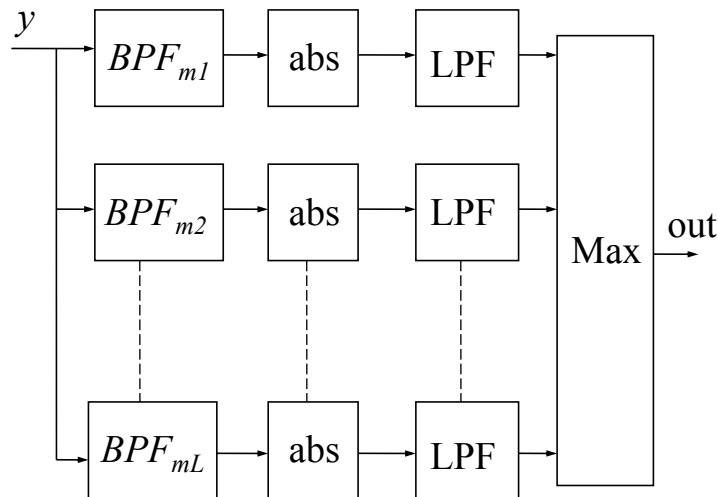


Figure 3.10. Filter bank system for the m^{th} mode.

Theoretically, a bank of fixed-parameter controllers needs to be implemented with one controller for each model in the model bank. Since each model only retains the plant natural frequency, and each fixed-parameter resonant controller only needs the natural frequency as a design parameter, then only one adjustable controller is used to replace the controller bank. At each sampling time the parameter ω_m of the closest model to the current plant is loaded into the adjustable controller through a switching system, as shown in Fig. 3.11.

To enable the multi-mode control, the above principle can be simply extended by replicating the filter bank system and the switching system repeatedly for all

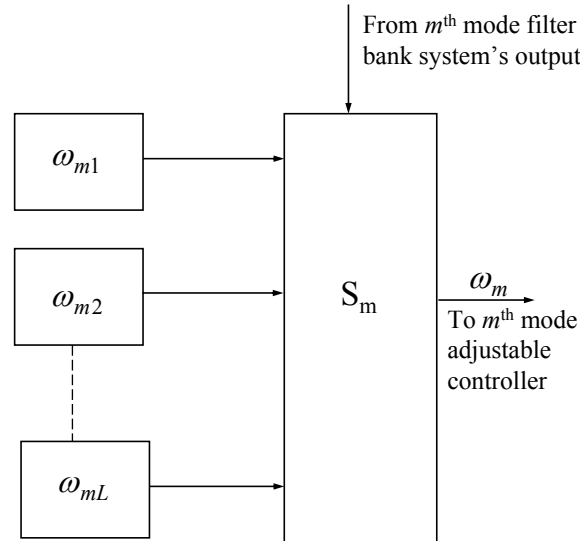


Figure 3.11. Switching system for the m^{th} mode.

the modes of interest. In this way the most appropriate models for all the modes of interest can be identified. A schematic diagram of the M⁴RC for M modes of interest is shown in Fig. 3.12.

Band-pass filter design

The complexity of the proposed supervisor scheme is significantly reduced relative to the complexity of the existing MMSE supervisor scheme. Only implementation of the BPF in the filter bank system is required in the design process of the proposed scheme. The centre frequency of the BPF is chosen to be the same as the natural frequency of each corresponding model. The pass-band of the BPF is chosen to be as narrow as possible so as to accurately represent the natural frequency of the model. However, to implement a very narrow pass-band, a high order filter is required. In the digital filter implementation, higher order filters require more memory and more computational time. Therefore, it is desirable to design a low order BPF with a narrow pass-band close to the filter centre frequency. To obtain a narrow low order BPF, a BPF with resonant controller structure is used in the filter bank of the M⁴RC. The BPF with resonant controller structure is a second-order filter which produces a sharper shape than the commonly used

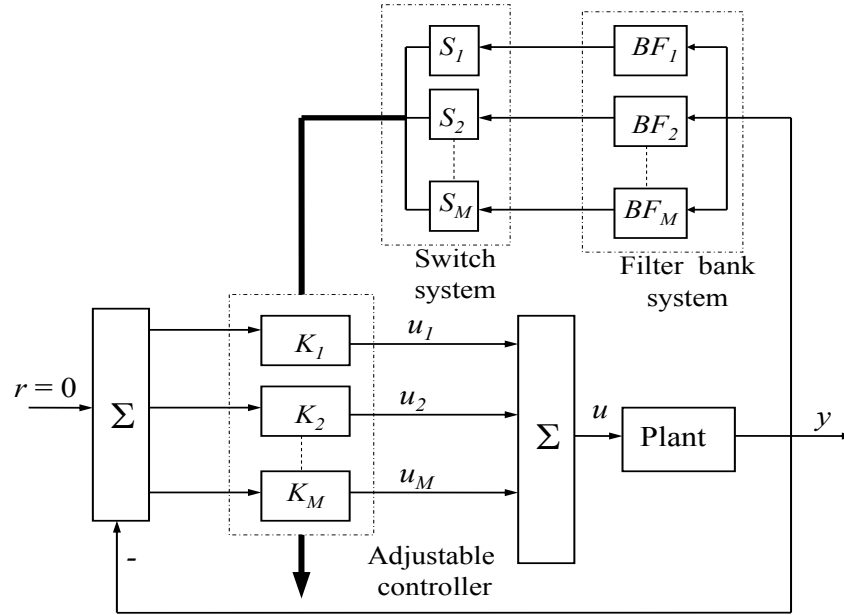


Figure 3.12. Block diagram of M^4RC for controlling M modes.

high order Butterworth filter. A comparison of the BPF with resonant controller structure ($k_c = 10$ and $\zeta_c = 0.01$) with Butterworth BPFs of different order is shown in Fig. 3.13. The figure shows that for frequencies close to the filter centre frequency, the BPF with resonant controller structure produces a sharper shape than a tenth-order Butterworth BPF.

Since the filter bank system selects the closest model that represents the current vibration frequencies at every sample time, it requires lower computational demand than the MMSE supervisor scheme. The new supervisor scheme only needs to determine which BPF produces the maximum output. Moreover, rapid switching does not occur in this scheme because the supervisor does not measure the error signal between the plant's output and the models' output, which could change rapidly, but instead uses the proximity of the plant natural frequencies to the fixed mode frequencies of the known models. Another advantage of the proposed supervisor scheme is that the parallel filter bank system can be easily embedded in a hardware system, which would reduce the computational time even more thus making it more suitable for real-time implementation.

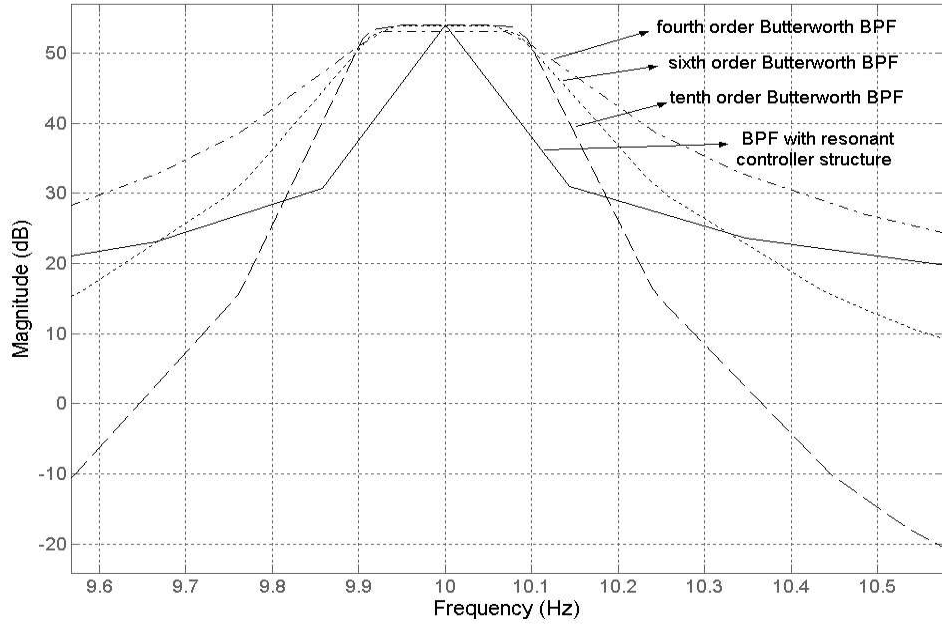


Figure 3.13: Comparative responses of BPF with resonant controller structure with Butterworth BPF.

The M⁴RC Algorithm

The algorithm for each mode is as follows:

1. Using the filter bank system select the BPF that gives the maximum output.
2. Load the parameters of the corresponding model into the adjustable resonant controller.
3. Calculate the control signal

$$u_m(k) = A_m y(k) + B_m y(k-1) + C_m y(k-2) - D_m u_m(k-1) - E_m u_m(k-2) \quad (3.39)$$

The final control signal is the summation of control signal for each mode

$$u(k) = \sum_{m=1}^M u_m(k) k_{dm}, \quad (3.40)$$

M⁴RC Stability

The multiple model control system using a supervisor scheme such as the M⁴RC can be categorized as a linear switched system. A linear switched system can be considered as a system that is composed of linear sub-systems. It is well-known that when all the linear systems which make up a switched system are stable, then the entire system is stable for any switching signal if the time between consecutive switching, known as the dwell time, τ , is sufficiently large [76, 156]. Furthermore, as stated in [100], the stability of multiple model control is guaranteed under the assumption that at every time there is at least one controller in the controller bank stabilize the system, and the interval between successive switches have a nonzero lower bound, which can be arbitrarily chosen to be small. For the proposed M⁴RC, stability is guaranteed because all the controllers in the controller bank stabilize the system and no rapid switching occurs between the controllers. To ensure stability an arbitrary small τ can be applied to the M⁴RC.

3.5.2 Case 2: Only the upper and Lower Bounds of Operating Region are *a priori* Known

Determining the number of required models needed to span an operating region in the multi-model control approach becomes a design problem if *a priori* knowledge about all the possible loading conditions is not available. The number of required models is determined by the bandwidth of the operating region and the choice of controller design. For a given bandwidth and operating region, a large number of models is required if narrow-band controllers are used, and fewer models are required if wide-band controllers are used.

The number of required models in the M⁴RC is very large due to the very narrow-band of the resonant controller, as demonstrated in the following illustrative example.

Example 3.5.1

Consider a resonant controller that is designed with an operating point at 10 Hz with a damping ratio $\zeta_c = 0.01$ and a gain $k_d = 10$. The frequency response of the controller is shown in Fig. 3.14. From the figure, it can be seen that the controller gain decreases by 15 dB for only a 0.05 Hz operating point variation. Assuming that a 15 dB reduction in the controller gain gives an acceptable closed-loop attenuation performance, then one model is required for every 0.1 Hz operating point variation, as shown in Fig. 3.15. As can be seen from Table 2.3, the operating regions for the physical plant under investigations are : 6 Hz - 10.5 Hz ; 44.8 Hz - 64 Hz ; 132.7 Hz - 174 Hz for the 1st, 2nd, and 3rd mode, respectively. Therefore, to span the operating region of the experimental plant the M⁴RC would require 45, 192, and 413 models for the 1st, 2nd, and 3rd mode, respectively or 650 models for the first three modes of vibration. The number of required models would increase for a tighter requirement (e.g., 5 dB reduction in the controller gain) or a wider operating region which would lead to a system with a very large number of models.

The example demonstrates that if only the lower and upper bounds of the operating region are *a priori* known in the M⁴RC method then a very large number of fixed-parameter models are required. A fast computer with lots of memory is required to implement such a control method. Therefore, the M⁴RC method is only practical for systems where all the loading conditions are *a priori* known. Simulation and experimental studies comparing the performance of the M⁴RC method for known loading conditions and for unknown loading conditions are reported in the following sections.

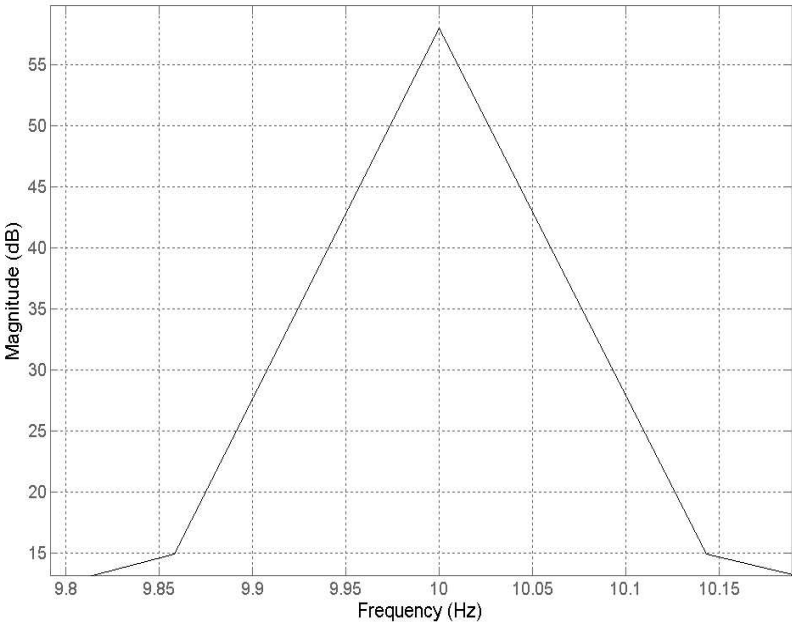


Figure 3.14: Frequency response of resonant controller with $\zeta_c = 0.01$ and $k_d = 10$.

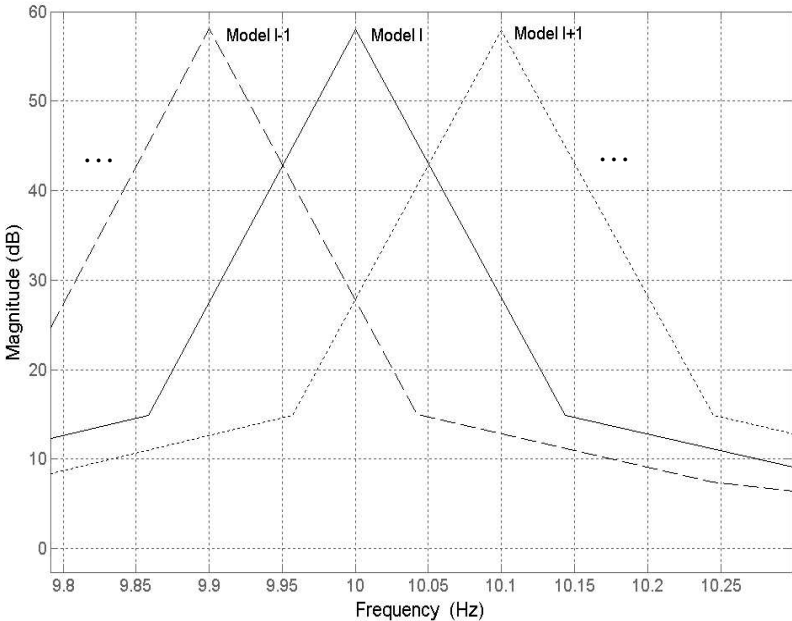


Figure 3.15. Model array in the M^4RC model bank.

3.6 Simulation Studies

In the following simulation studies, the resonant control method and the M⁴RC method are applied to control the cantilever beam when loaded with the various loads (Model 1 to Model 4), as described in Chapter 2.

The objectives of the first simulation study (3.6.1) of the resonant control method are to demonstrate that:

1. Resonant control is able to attenuate multi-mode vibration using only a single sensor-actuator pair.
2. Resonant control has an independent characteristic, in the sense that the controller is able to control a particular mode without destabilising the other modes.
3. Resonant control fails to give optimum performance when the natural frequencies of the system are altered due to load changes.

The objective of the second simulation study (3.6.2) is to demonstrate that:

1. The proposed M⁴RC supervisor scheme does avoid rapid switching.
2. The proposed M⁴RC supervisor scheme has a reduced computational demand vis-a-vis a multiple model control system using the MMSE supervisor scheme (3.35) [6, 38, 75].

3.6.1 Resonant Controller

The resonant controller (3.6) is used to control the first three vibration modes of simulation models. The parameters of the controller are chosen as $k_{d1} = k_{d2} = k_{d3} = 10$ and $\zeta_{c1} = \zeta_{c2} = \zeta_{c3} = 0.01$ through a trial and error process. Six simulation cases, referred to as RC.1 to RC.6, are conducted in this study. In

the RC.1 to RC.4 cases, controllers that are specifically designed for Model 1 to Model 4 are used to control each corresponding model. These cases are designed to test the performance of the resonant controller's ability to attenuate multi-mode vibration when the controller centre frequencies match the natural frequencies of the plant. The RC.5 case is similar to the RC.1 case, however, only the controller for the second mode is activated by setting $k_{d1} = k_{d3} = 0$. The objective of the RC.5 case is to demonstrate the capability of the resonant controller to independently attenuate a single mode for multi-mode excitation. In the RC.6 case, a controller that is specifically designed for Model 3 is used to control the system where the loading conditions change from Model 1 \rightarrow 3 \rightarrow 4. This case is designed to test the performance of the controller when the natural frequencies of the plant vary due to changes in the plant's loading. The configurations of the plant and the controller for all the cases are shown in Table 3.2. The excitation signal for all cases is a summation of three 1 volt sinusoidal signals representing the first three natural frequencies of the particular model.

Case	Loading condition represented by Model	Controller design based on Model
RC.1	1	1
RC.2	2	2
RC.3	3	3
RC.4	4	4
RC.5	1	1*
RC.6	1 \rightarrow 3 \rightarrow 4	3
* only the 2 nd mode controller is activated		

Table 3.2: Plant and controller configurations for resonant controller simulation study.

RC.1 to RC.4 cases

The system responses and the control signals for cases RC.1 to RC.4 are shown in Figs. 3.16 to 3.19. From the figures it can be seen that the resonant control is able to attenuate multi-mode vibration using only a single sensor-actuator pair.

The attenuation level for the different models is shown in Table 3.3, and the attenuation of each mode for all the different models are shown in Figs. 3.20 to 3.23. The figures show that for each model and for each mode the attenuation level is different. These differences in levels of attenuation are attributable to the sensitivity of the sensor to the different vibration modes and the authority of the actuator in attenuating the same modes, which are in-turn determined by the position of the sensor-actuator pair along the beam. It is observed in Chapter 2 that positioning the sensor close to the cantilevered end makes the sensor most sensitive to the second mode vibration. Similarly due to the collocated position of the sensor and actuator, the control authority for the second mode is at its highest.

	Attenuation (dB)			
	mode 1	mode 2	mode 3	overall
Model 1	10.0	17.8	17.2	19.7
Model 2	15.2	22.3	20.3	23.9
Model 3	17.2	19.9	16.2	21.4
Model 4	18.9	31.5	23.6	30.3

Table 3.3. Attenuation level for the range of models.

RC.5 case

The response of the system in the frequency domain for the RC.5 case is shown in Fig. 3.24. From the figure it can be seen that the resonant controller produces the same attenuation as the RC.1 case for the second mode but gives no attenuation or amplification for the other two modes. The result shows that the resonant controller is capable of attenuating specific modes independently of the other modes, which is an advantage for certain applications where only specific modes need to be controlled.

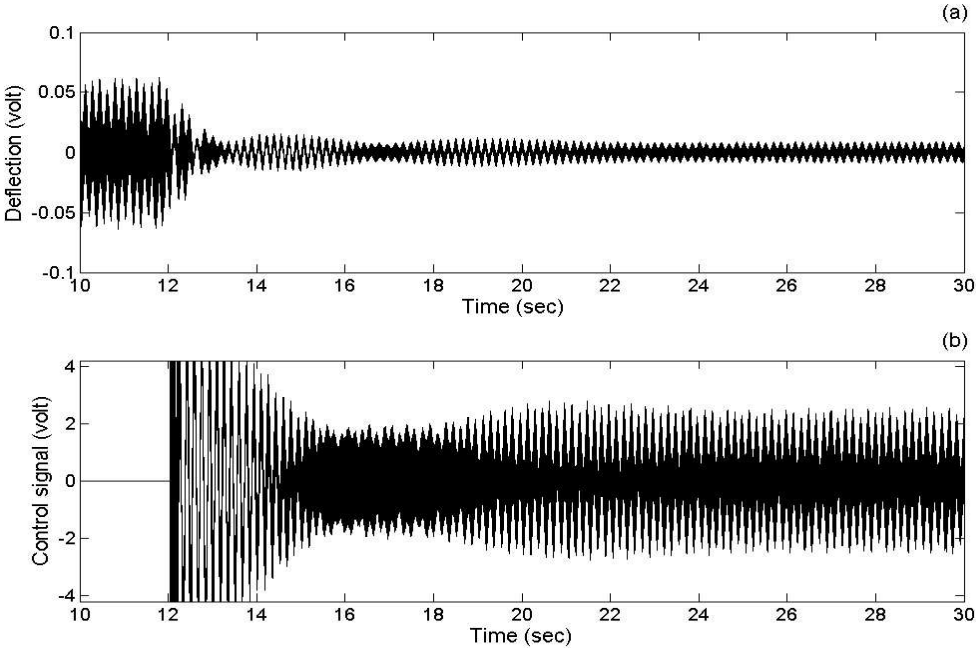


Figure 3.16: Response of Model 1 and the corresponding control signal.

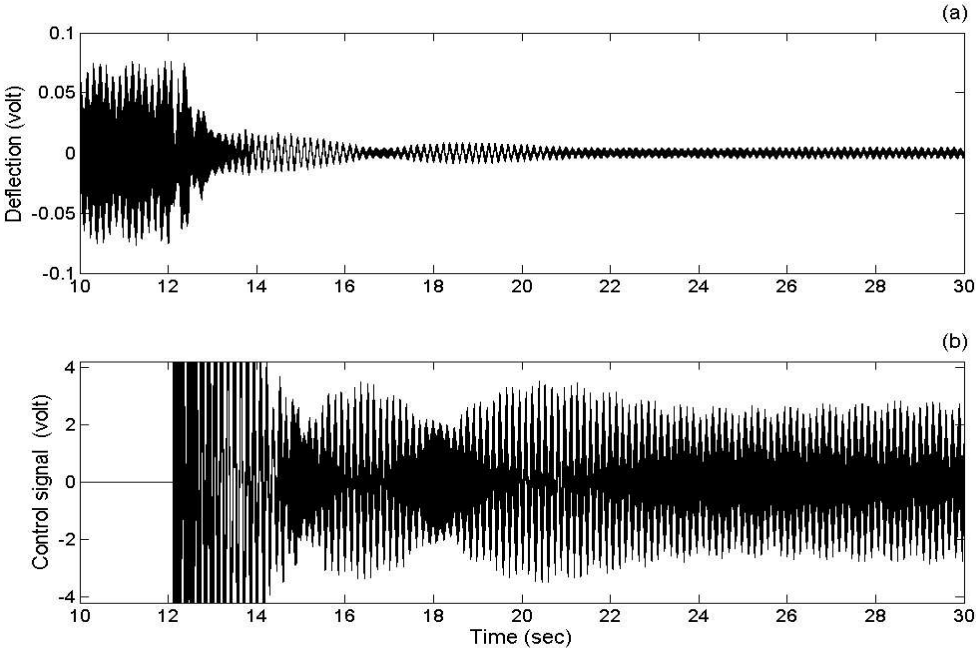


Figure 3.17: Response of Model 2 and the corresponding control signal.

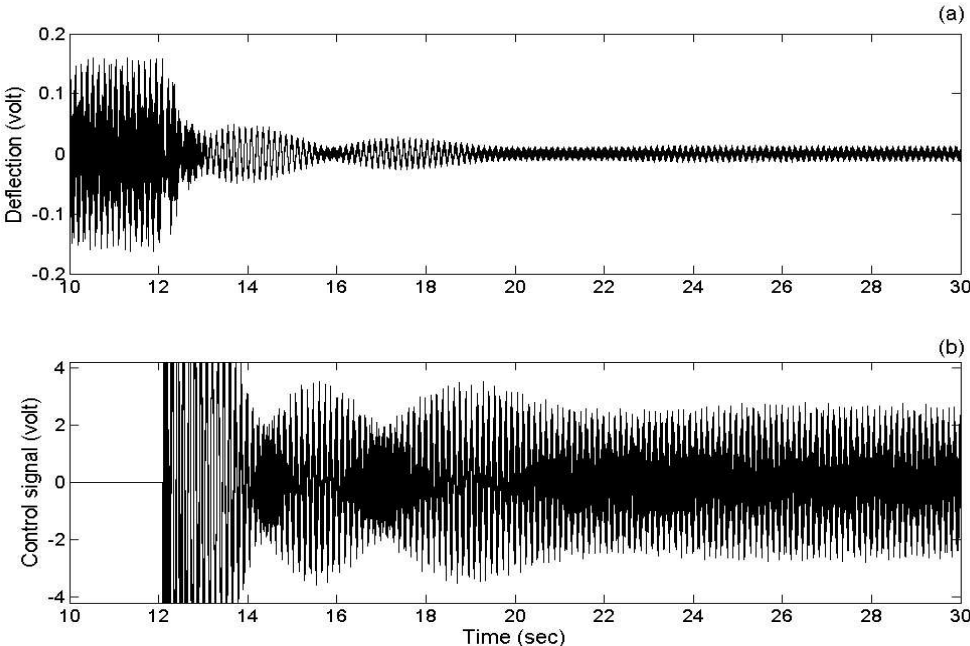


Figure 3.18: Response of Model 3 and the corresponding control signal.

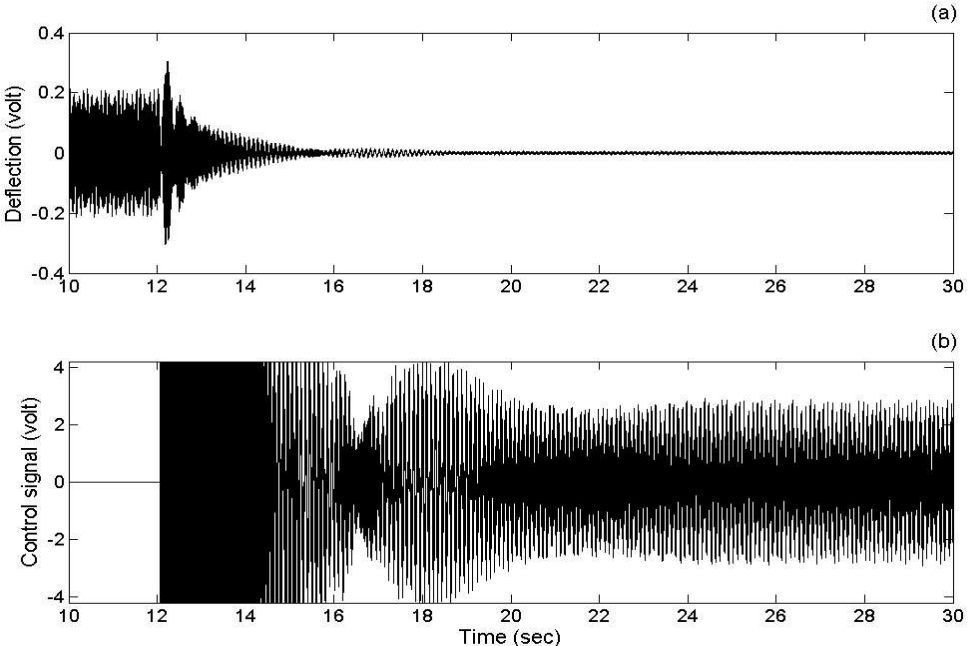


Figure 3.19: Response of Model 4 and the corresponding control signal.

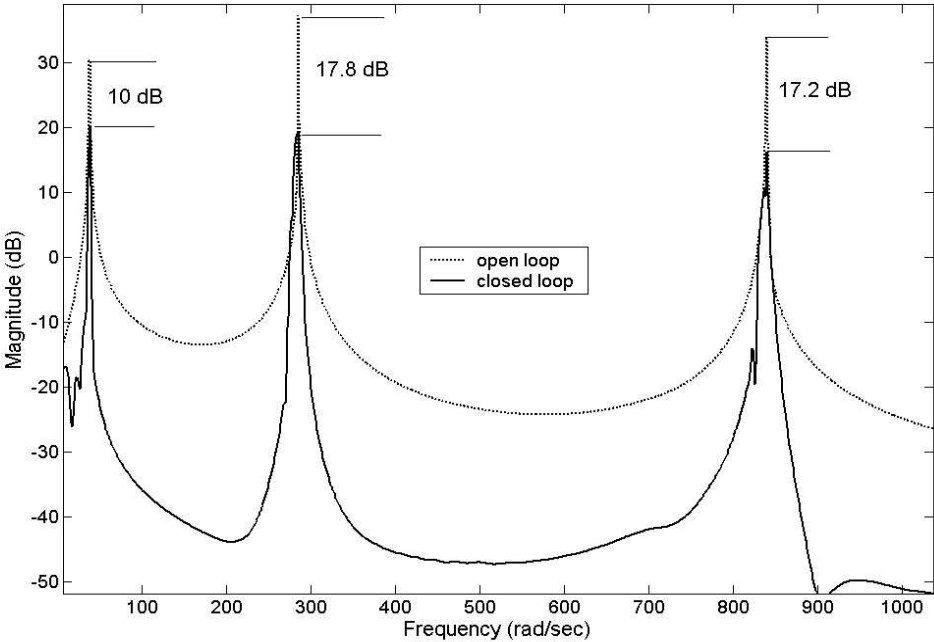


Figure 3.20. Frequency response of Model 1.

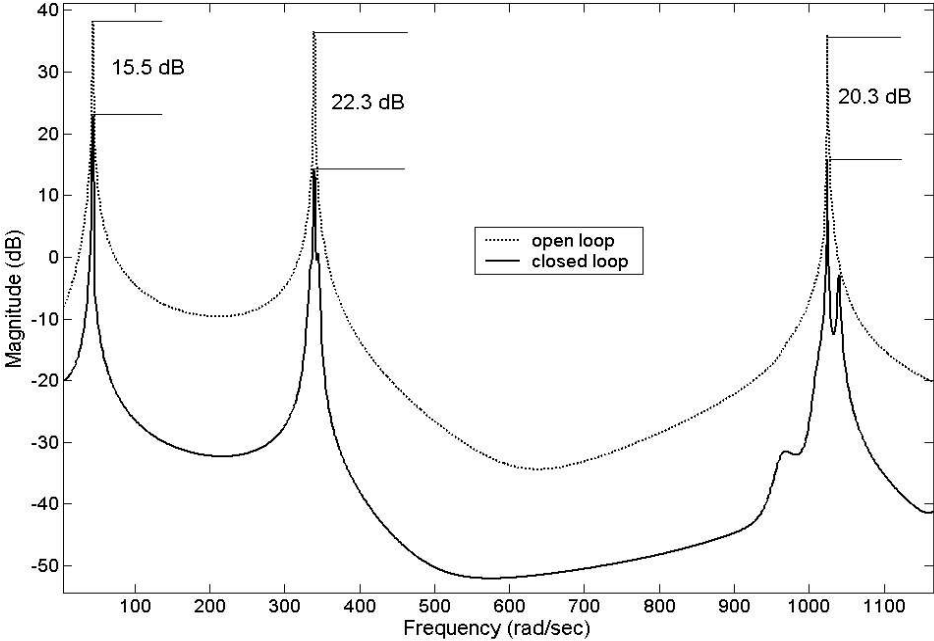


Figure 3.21. Frequency response of Model 2.

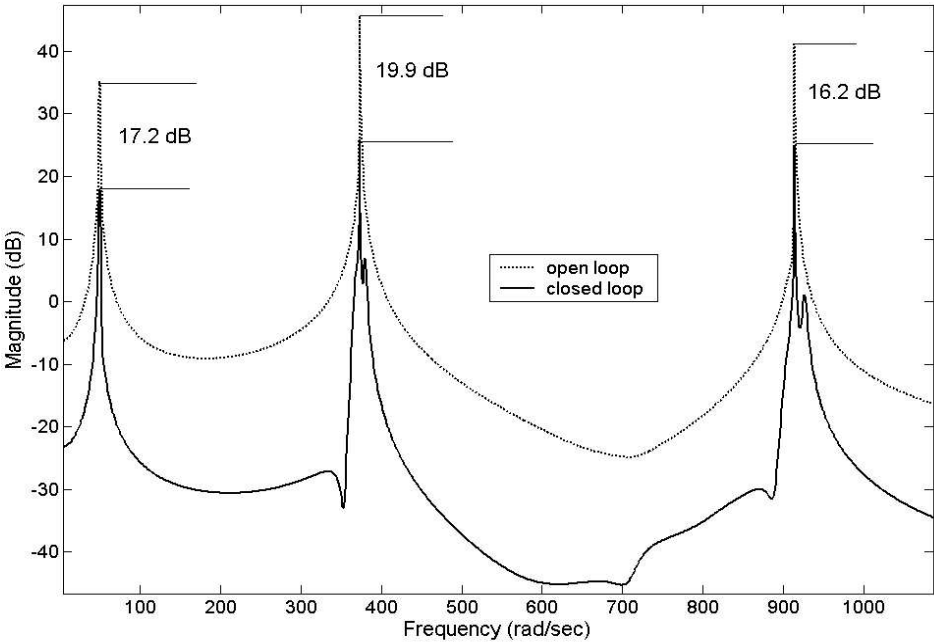


Figure 3.22. Frequency response of Model 3.

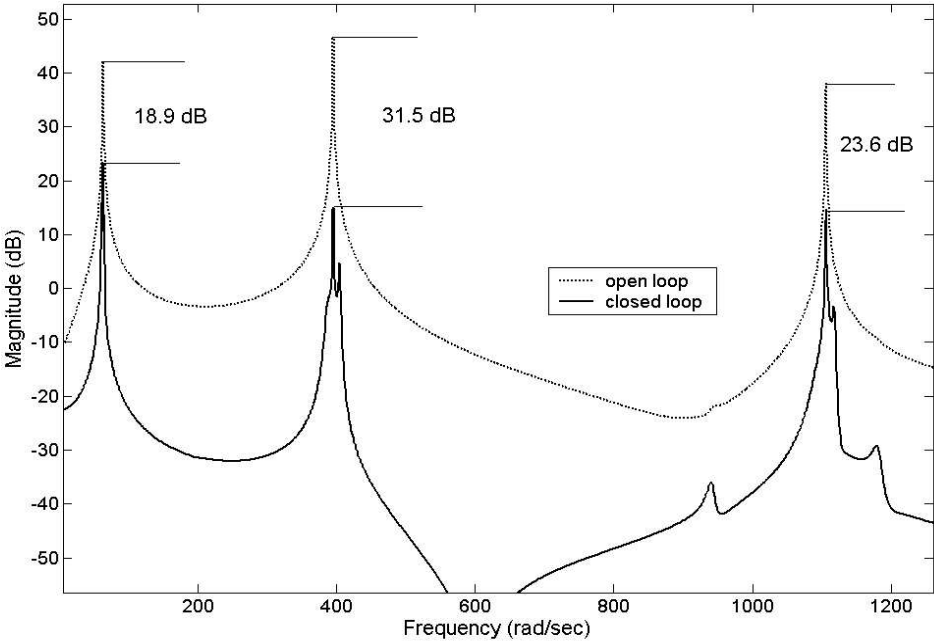


Figure 3.23. Frequency response of Model 4.

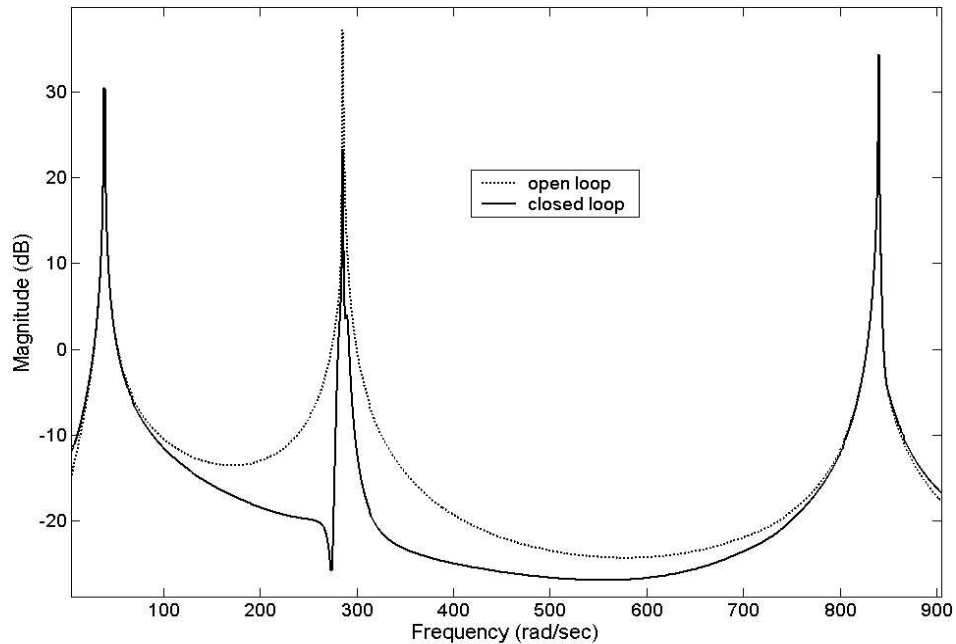


Figure 3.24: Frequency response of Model 1 with only the 2nd mode controller active.

RC.6 case

In the RC.6 case, the loading condition changes from Model 1 to Model 3 at $t = 30$ seconds, and to Model 4 at $t = 60$ seconds. The open-loop and closed-loop time domain responses of the system are shown in Fig. 3.25 and Fig. 3.26, respectively. From the comparison of the two figures, it can be seen that between $t = 30$ and $t = 60$ when the system loading condition is represented by Model 3, the controller gives a good performance with 21.4 dB attenuation. However, when the system loading conditions are represented by either Model 1 or Model 4, although the system is stable, the controller gives poor attenuation performance with only 0.7 dB and 8.7 dB attenuation, respectively. When the Model 1 loading condition is used, the controller only produces a maximum amplitude control signal of around 0.3 volts, as shown in Fig. 3.26(b). Since this control signal only generates a small force at the actuator, only a small amount of attenuation is

achieved. When the Model 4 loading condition is used, the controller produces a maximum amplitude control signal of around 3 volts. However, due to mismatches between the controller centre frequencies and the natural frequencies of the system under control, optimum attenuation cannot be achieved. Therefore, it can be evident that the resonant controller is sensitive to unforeseen changes in the natural frequencies of the system for which it was not designed and for which it could not compensate. In the next subsection, it will be shown that the multiple model resonant controller is able to give better performance than the single model resonant controller for systems with varying natural frequencies.

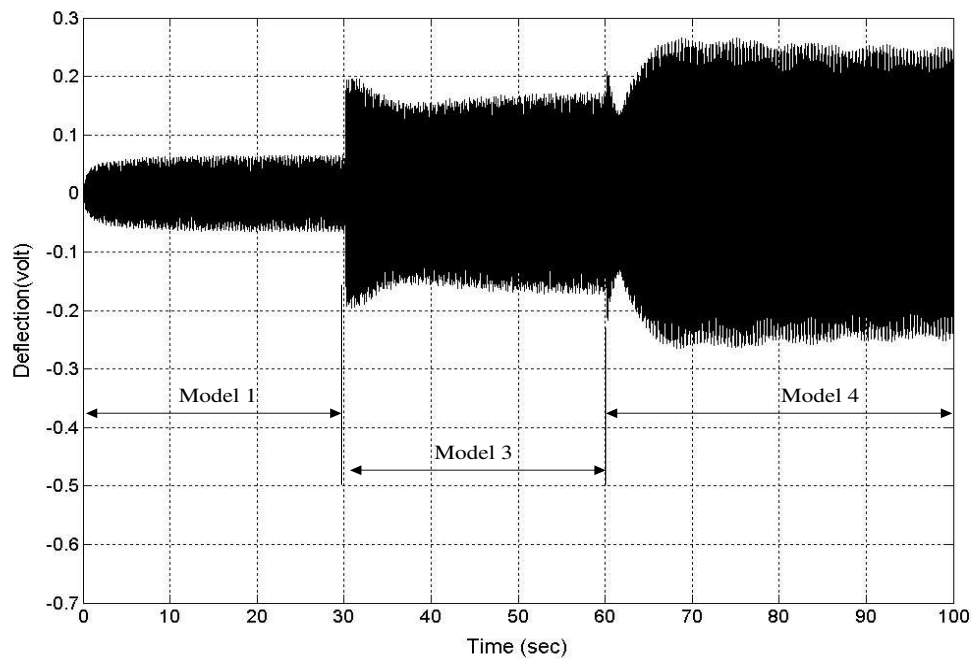


Figure 3.25: Open-loop system response for the 1 \rightarrow 3 \rightarrow 4 model sequence.

3.6.2 M⁴RC

To control the first three modes of vibration, the proposed multiple model resonant control uses three sets of filter banks (BF_1 , BF_2 , and BF_3), one for each

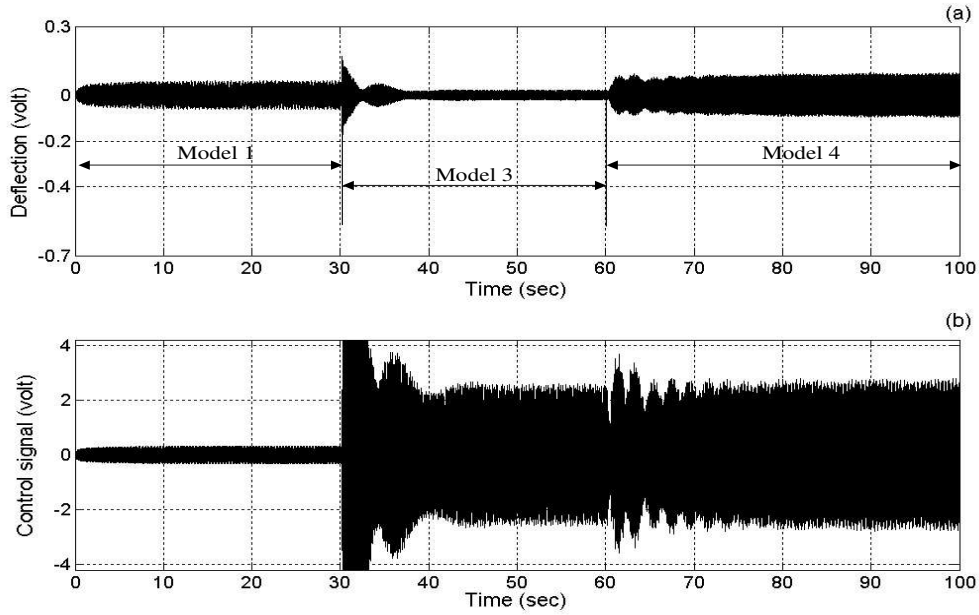


Figure 3.26: Closed-loop system response for the 1 → 3 → 4 model sequence.

mode of vibration. The band-pass filters (BPFs) in the filter bank are implemented as BPFs with a resonant controller structure. The centre frequency of each filter is set according to the frequencies of the corresponding first 3 modes of Model 1, Model 3 and Model 4, respectively. The performance of the proposed M⁴RC supervisor scheme is compared with that of the MMSE supervisor scheme (3.35). To give balance to both instantaneous and long-term measurement accuracy, the parameters α and β are chosen to have the same value. A moderate value of λ is chosen to accommodate both disturbances and sudden changes. A moderate value of λ should avoid unwanted switching due to disturbances in the system and yet be fast enough to follow sudden changes in the system parameters. Based on this reasoning, the supervisor scheme is implemented with $\alpha = \beta = 1$ and $\lambda = 0.5$, and the performance index is computed for every 100 samples. The model bank includes three models, Model 1, Model 3, and Model 4 where each model is of order 20, as obtained in Chapter 2. The controllers' parameters k_{di}

and ζ_{ci} are the same as those of the resonant controller described in the previous subsection. The schematic diagrams of the implemented M⁴RC and of the multi-model control with the MMSE supervisor scheme are shown in Fig. 3.27 and Fig. 3.28, respectively.

Two simulation cases referred to as M⁴RC.1 and M⁴RC.2 are tested. The loading sequences and the controllers configurations for both cases are shown in Table 3.4. The loading conditions in both cases are changed at $t = 5$ seconds and $t = 15$ seconds.

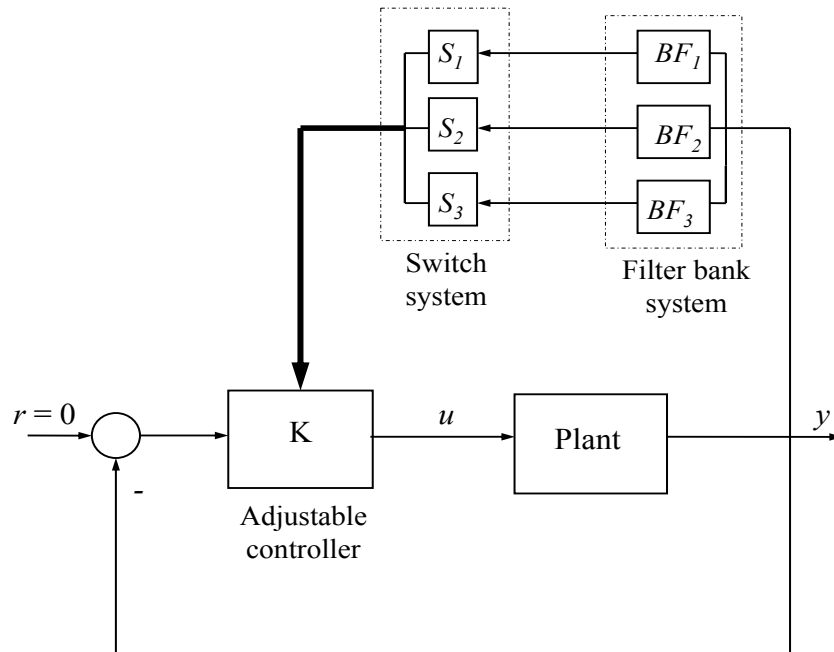


Figure 3.27. Schematic diagram of the implemented M⁴RC.

Case	Loading condition is represented by Model	Models in the model bank are based on Model
M ⁴ RC.1	1→3→4	1,3,4
M ⁴ RC.2	1→2→4	1,3,4

Table 3.4: Plant and controller configurations for M⁴RC simulation study.

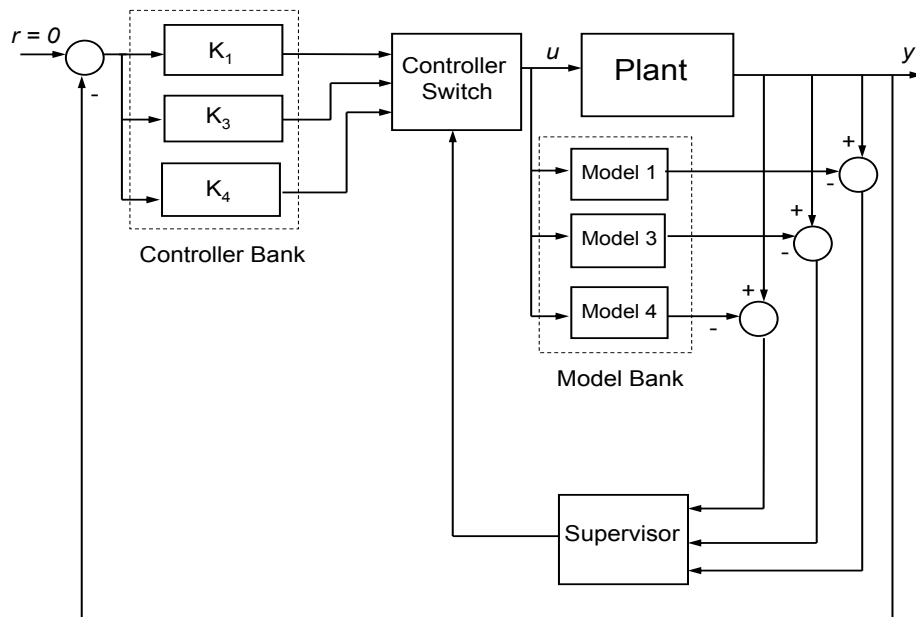


Figure 3.28: Schematic diagram of the multi-model control with MMSE supervisor scheme.

$M^4RC.1$ case

For the $M^4RC.1$ case, all the loading conditions are represented in the model bank. In this case, both supervisor schemes select the appropriate controller corresponding to the current loading condition, as can be seen from the switching behaviour shown in Figs. 3.29 (a) to (f). Fig. 3.30 shows that both supervisor schemes give similarly good attenuation performance. This result confirms that if the assumption that all the loading conditions are *a priori* known is satisfied, then the proposed supervisor scheme will select the appropriate controller, and the system performance will be optimum, similar to the more complex MMSE supervisor scheme.

$M^4RC.2$ case

For the $M^4RC.2$ case, Model 2 is not included in the model bank. As the loading condition changes to Model 2, rapid switching occurs between all the controllers in the controller bank when using the MMSE supervisor scheme. The rapid switching shown in Figs. 3.31(a) to (c) leads the controller to produce a satu-

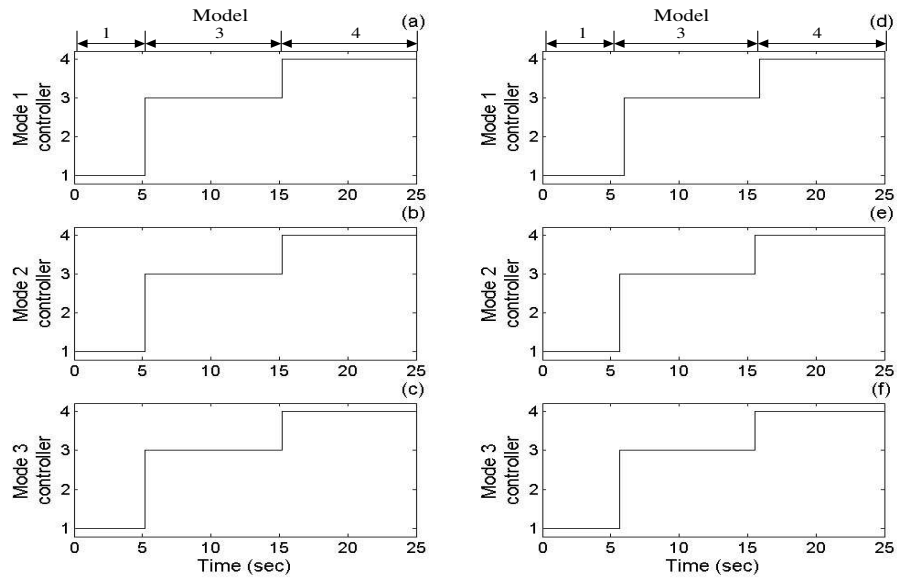


Figure 3.29: M^4RC switching behaviour for the $1 \rightarrow 3 \rightarrow 4$ model sequence. (a)-(c) using MMSE supervisor scheme for mode 1, 2 and 3 respectively. (d)-(f) using proposed supervisor scheme for mode 1, 2 and 3 respectively.

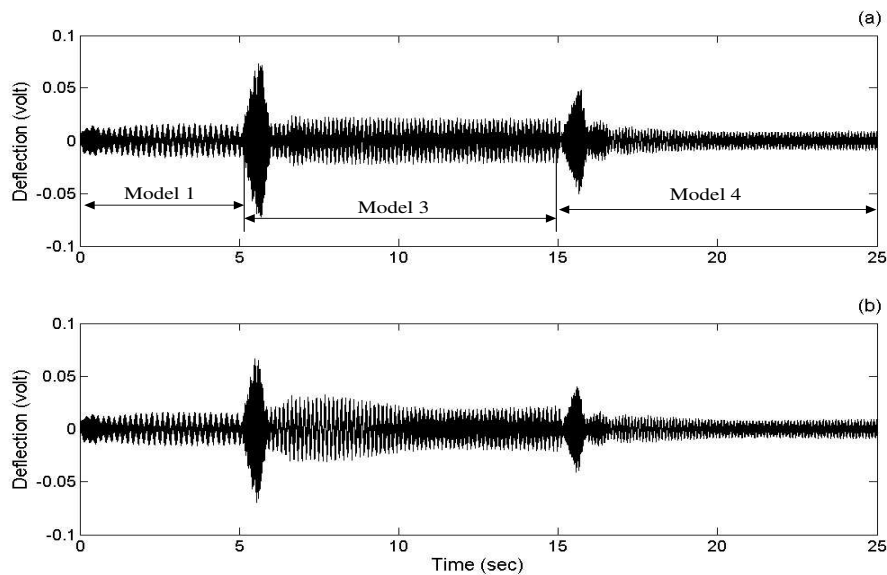


Figure 3.30: Closed-loop multiple model resonant control responses for the $1 \rightarrow 3 \rightarrow 4$ model sequence. (a) using MMSE supervisor scheme. (b) using proposed supervisor scheme.

rated control signal as shown Fig. 3.32(a), resulting in poor performance. The controller amplifies the vibration during the period 9 to 14 seconds as shown in Fig. 3.33 (a). Conversely, rapid switching does not occur for the M⁴RC using

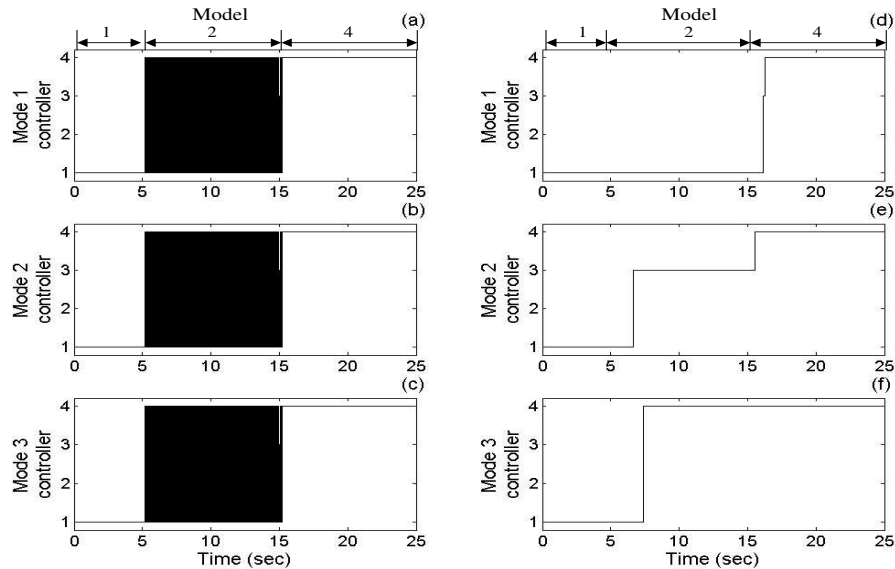


Figure 3.31: M⁴RC switching behaviour for the 1 → 2 → 4 model sequence. (a)-(c) using MMSE supervisor scheme for mode 1, 2 and 3 respectively. (d)-(f) using proposed supervisor scheme for mode 1, 2 and 3 respectively.

the proposed supervisor scheme. Instead, the supervisor chooses the model with the closest natural frequencies to the excitation signal when the exact model is not in the model bank. Due to the values of the models' natural frequencies, as shown in Table 2.6, when the loading condition changes to Model 2 the supervisor chooses Controller 1, Controller 3 and Controller 4 for mode 1, mode 2, and mode 3, respectively, as shown in Figs. 3.31 (d) to (f). In this way, although the controller cannot give optimum performance for the unknown Model 2, it still gives 3.64 dB attenuation as shown in Fig. 3.33(b).

Relative to the MMSE supervisor scheme, the proposed supervisor requires less computational time. With three models in the model bank, the actual time

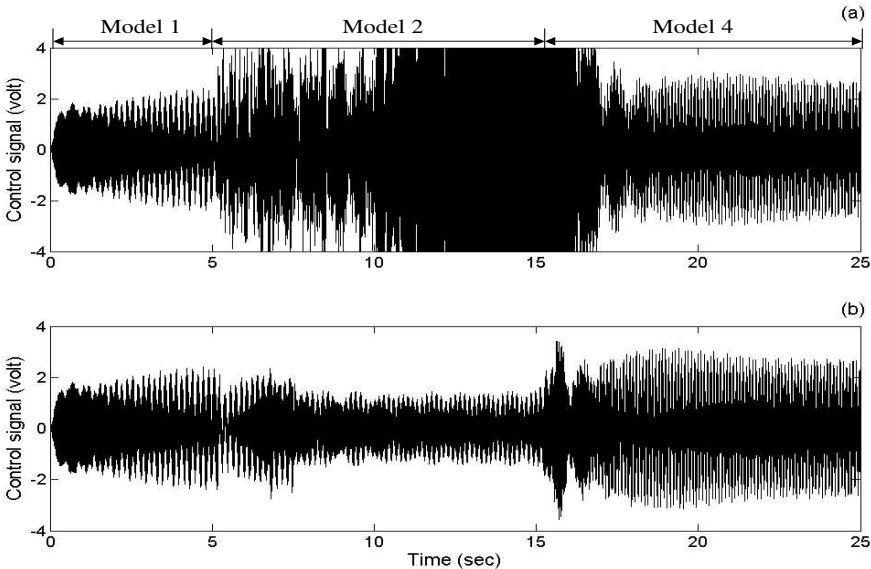


Figure 3.32: Control signals generated by the multiple model resonant control for the $1 \rightarrow 2 \rightarrow 4$ model sequence. (a) using MMSE supervisor scheme. (b) using proposed supervisor scheme.

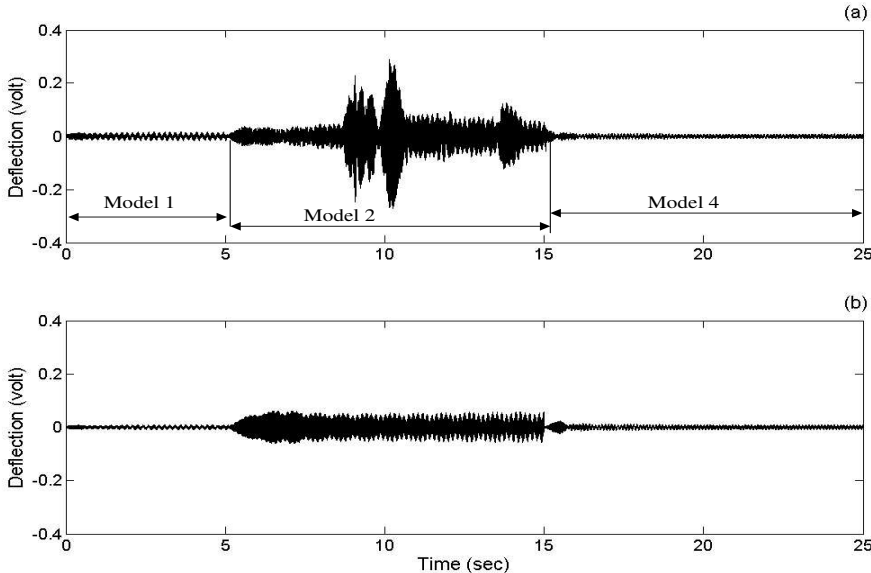


Figure 3.33: Closed-loop responses of multiple model resonant control for the $1 \rightarrow 2 \rightarrow 4$ model sequence. (a) using MMSE supervisor scheme. (b) using proposed supervisor scheme.

required to compute 25 seconds of simulation time is 100 seconds using the MMSE supervisor scheme compared to only 50 seconds using the proposed supervisor scheme. In the MMSE supervisor scheme, the time needed for the computation will significantly increase as the number of models increase, as mentioned in Section 3.4. In the case of the proposed supervisor scheme, increasing the number of models will only increase the number of band-pass filters without significantly increasing the time needed to compute which band-pass filter gives the maximum output. The difference in the computation times between the two supervisor schemes shows that for the real-time implementation, the proposed supervisor scheme is more practical than the MMSE supervisor scheme.

3.7 Experimental Studies

Experimental studies are used to verify the results of the simulation studies. The resonant controller and the proposed multiple model resonant controller are implemented on a dSPACETM DS1103 data acquisition and control board using MatlabTM, SimulinkTM and Real-Time WorkshopTM software. The schematic diagram of the experimental set-up is shown in Fig. 3.34. The power supply drives the coils that hold the loads to the beam through a switch box. Since the maximum output voltage from the digital to analogue converter (DAC) in the dSPACE is 5 volts and the maximum allowable voltage to be applied to the piezoactuator is 100 volts, a piezo power amplifier with a gain of 20 is used to drive the piezoactuator. The output signal from the piezosensor which has a maximum amplitude in order of 500 volts is divided by 100 using a differential probe before feeding it back to the analogue to digital converter (ADC) in the dSPACE board. As a precaution, and so as not to break the piezoactuator, the voltage applied to the piezoactuator is limited to ± 80 volts. Therefore, a saturation block with a maximum and a minimum output ± 4 is added to the controller's output to

limit the control signal. In the experiment, the control signal and the disturbance signal are applied to the system through the same piezoactuator. All the filter and controller parameters are the same as those used for the simulation studies in the previous section. Similarly to the simulation studies two sets of experimental studies are conducted, one using the resonant controller and the other using the multiple model resonant controller.

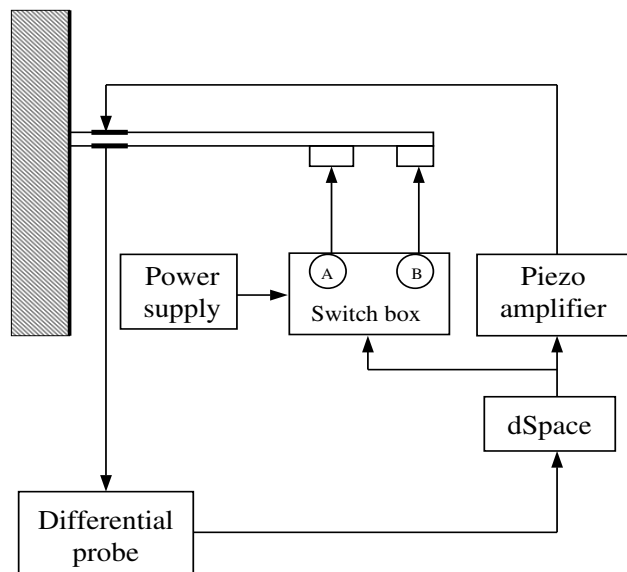


Figure 3.34. The experimental set-up.

3.7.1 Resonant Controller

The same protocol is followed for the physical experiments as for the simulation studies in Section 3.6.1. Once again, six experimental cases, RC.1 to RC.6, as shown in Table 3.2 are conducted.

RC.1 to RC.4 cases

For the RC.1 to RC.4 cases, the system responses and the control signals in the time domain are shown in Figs. 3.35 to 3.38, and the system responses in

the frequency domain are shown in Figs. 3.39 to 3.42. The figures show good agreement with the simulation results. The attenuation levels for the different models are shown in Table 3.5.

	Attenuation (dB)			
	mode 1	mode 2	mode 3	overall
Model 1	14.0	23.3	12.0	21.0
Model 2	17.6	20.8	18.2	25.1
Model 3	16.7	24.8	20.2	24.4
Model 4	22.6	27.3	21.4	30.5

Table 3.5. Attenuation level for the range of models.

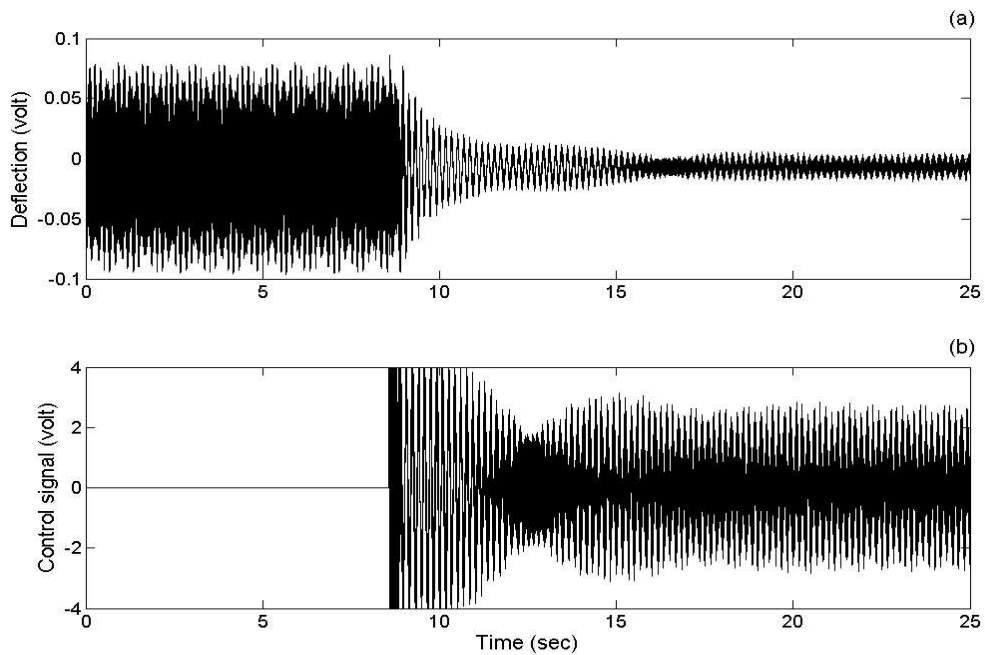


Figure 3.35: Response of Model 1 and the corresponding control signal.

RC.5 case

The frequency response of the system for the RC.5 case, as shown in Fig. 3.43, confirms that the resonant control is able to control a specific mode of vibration without destabilizing uncontrolled modes.

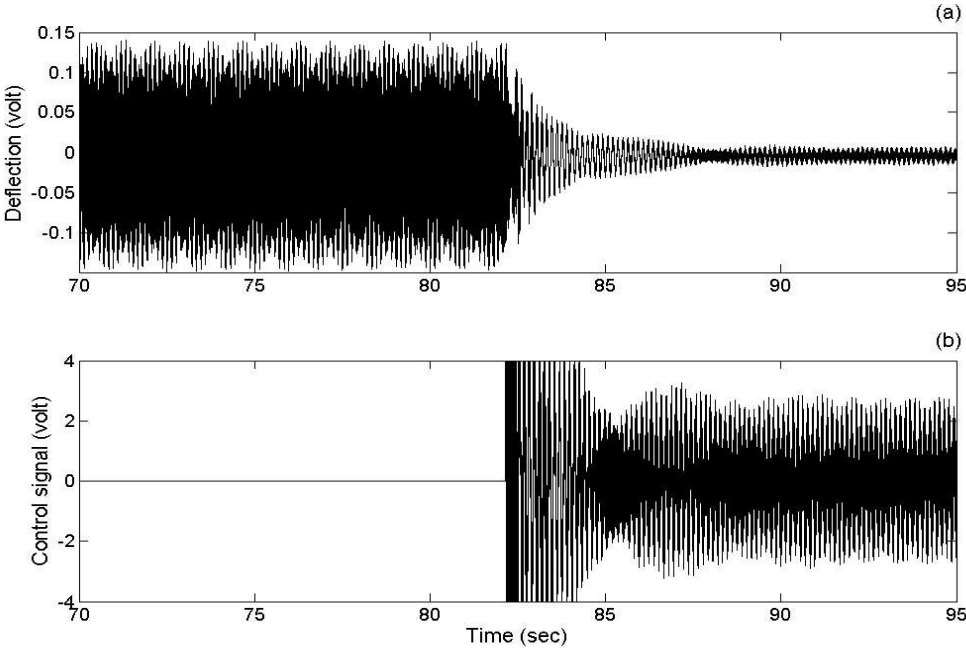


Figure 3.36: Response of Model 2 and the corresponding control signal.

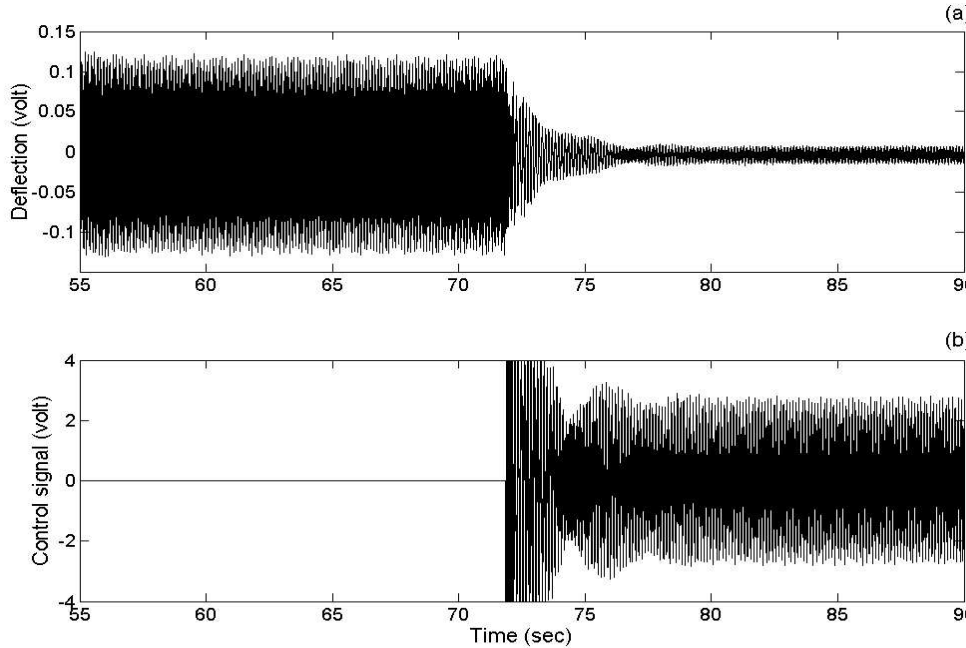


Figure 3.37: Response of Model 3 and the corresponding control signal.

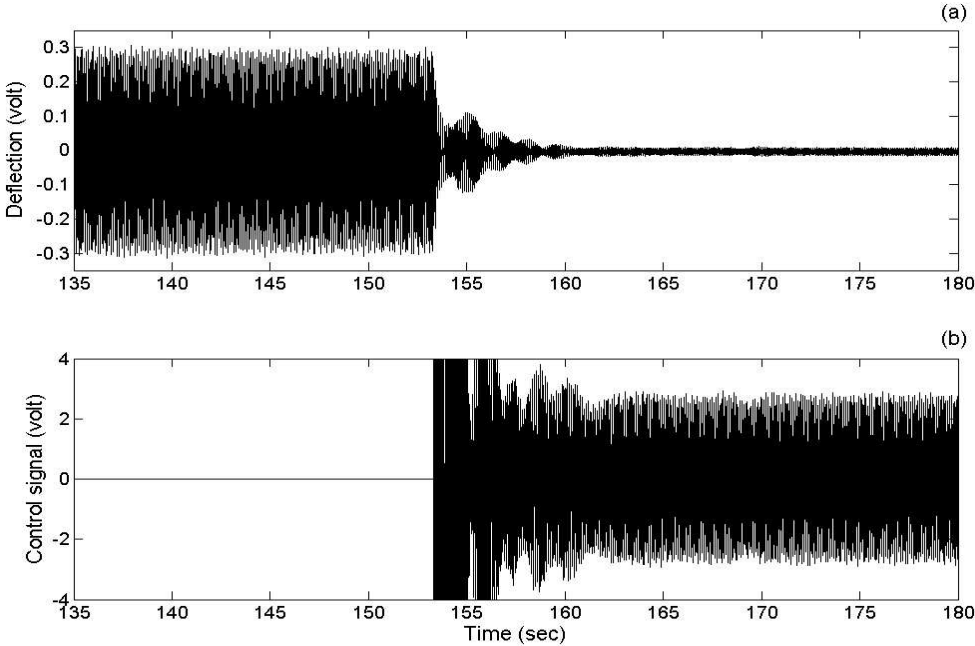


Figure 3.38: Response of Model 4 and the corresponding control signal.

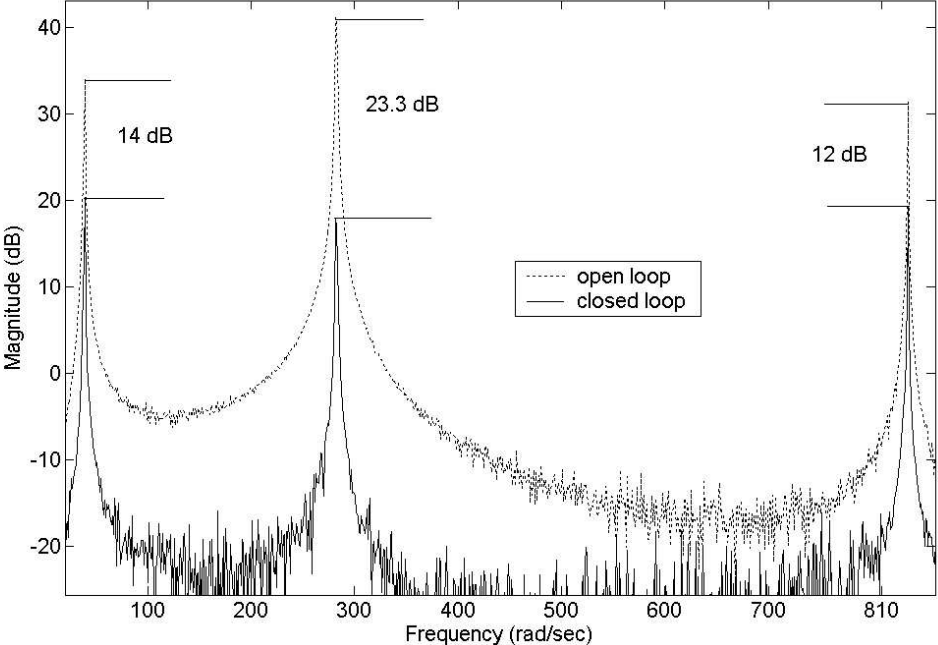


Figure 3.39. Frequency response of Model 1.

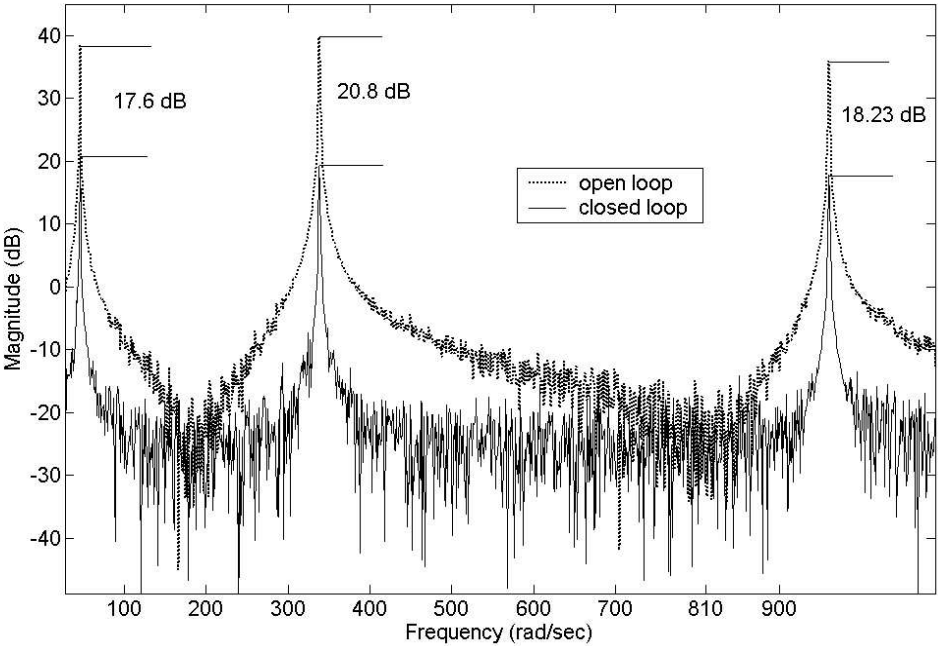


Figure 3.40. Frequency response of Model 2.

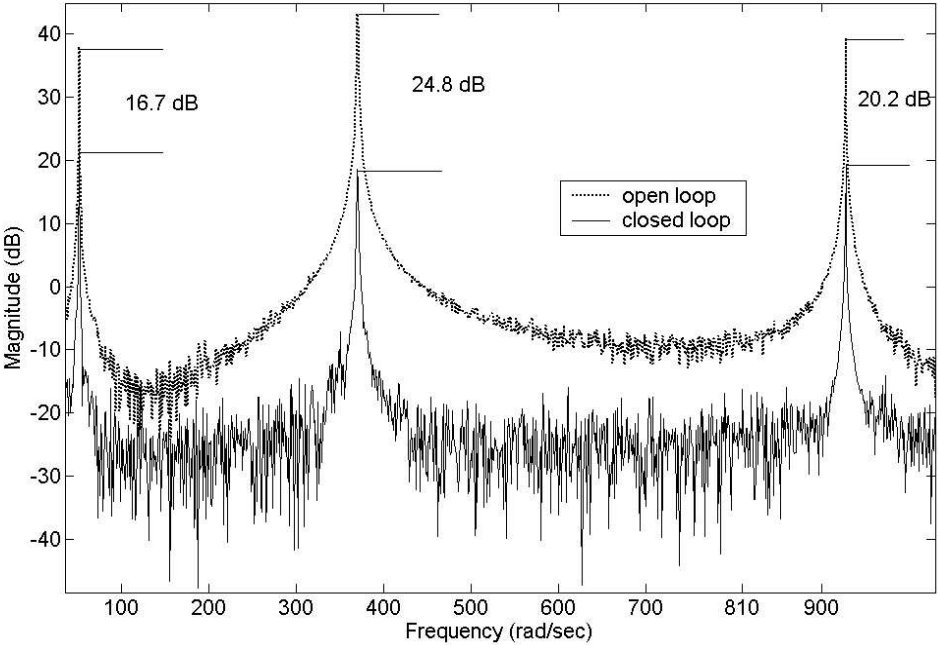


Figure 3.41. Frequency response of Model 3.

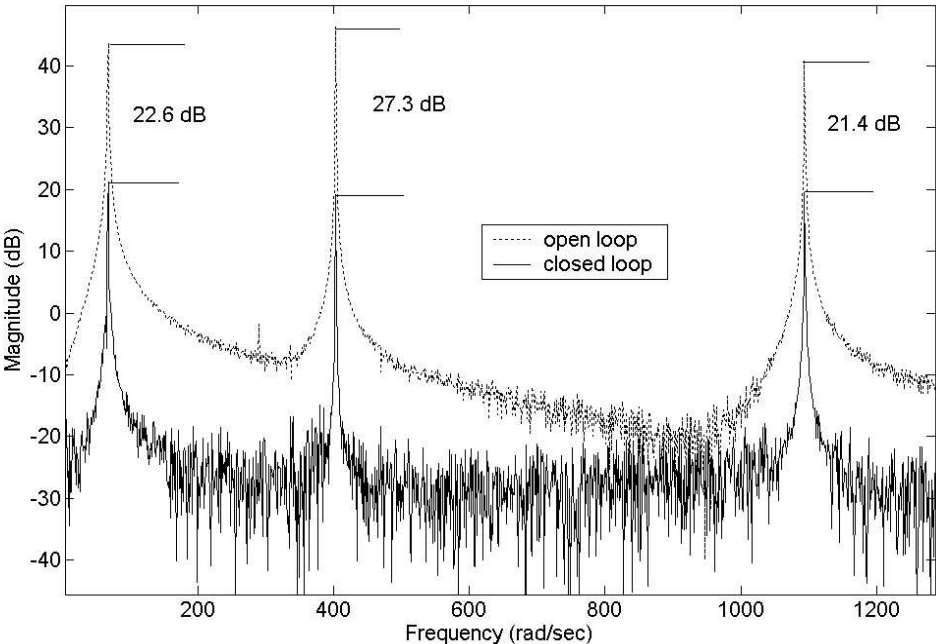


Figure 3.42. Frequency response of Model 4.

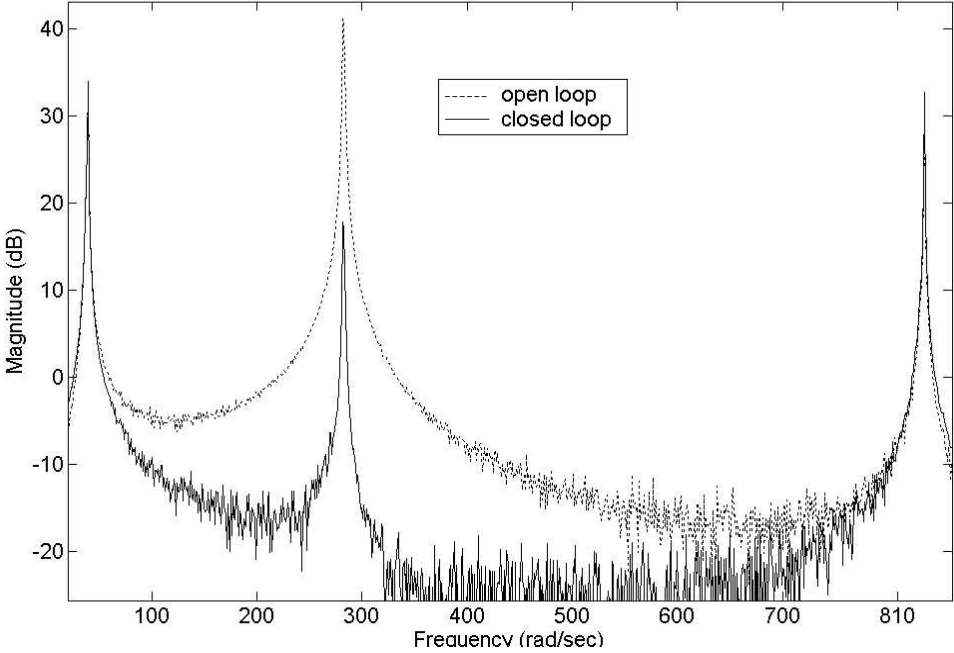


Figure 3.43: Frequency response of Model 1 with only the 2nd mode controller active.

RC.6 case

For the RC.6 case, the open loop response of the system, when the system changes from one loading condition to the next, is shown in Fig. 3.44. The figure shows that there is good agreement with the corresponding simulation result. However, the experiment result shows that there is a peak in the downward direction when the system changes from one loading condition to the next. The explanation for this phenomenon is that releasing a load is equivalent to applying a pulse of force which causes a large non-symmetric oscillation. The amplitude of the upward oscillation is smaller because the force of gravity makes the upward resultant force smaller than the downward resultant force. The closed-loop response and the control signal for the system are shown in Fig. 3.45. This figure also shows that there is good agreement with the corresponding simulation result.

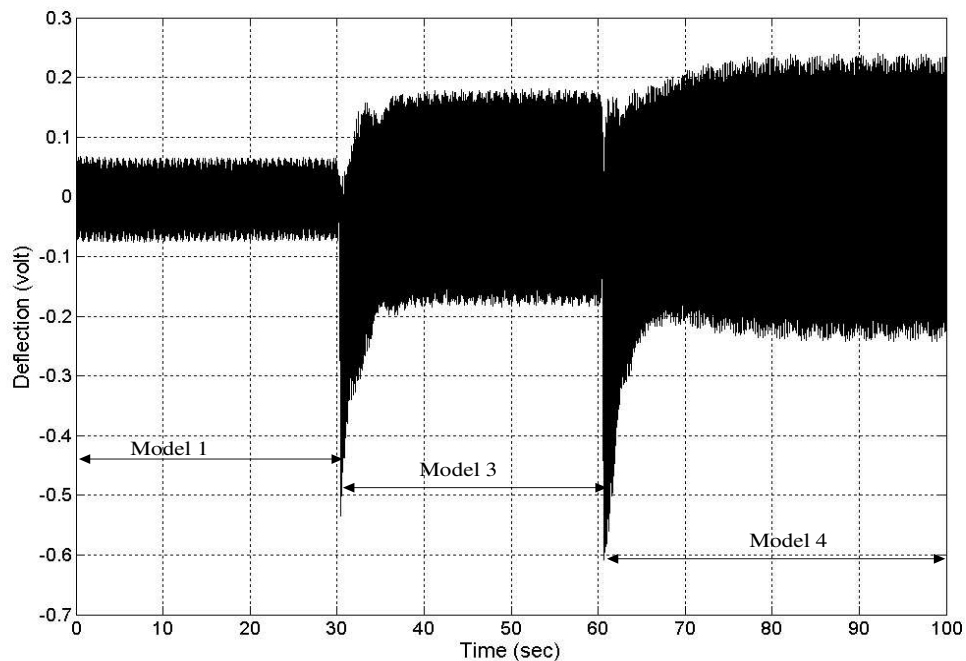


Figure 3.44: Open-loop system response for the 1 \rightarrow 3 \rightarrow 4 model sequence.

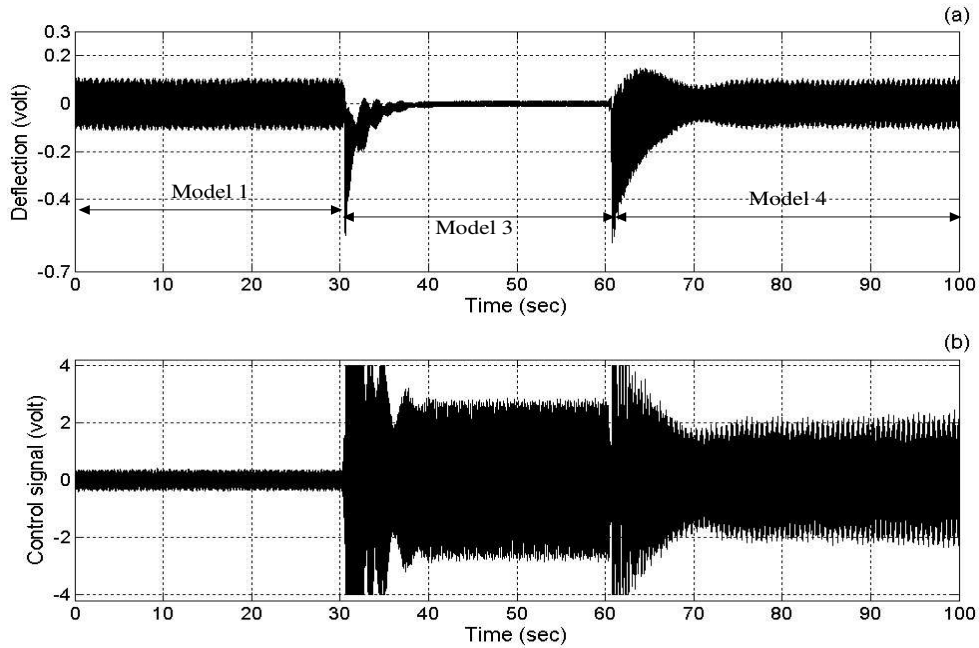


Figure 3.45: Closed-loop system response for the $1 \rightarrow 3 \rightarrow 4$ model sequence with the controller designed based on Model 3.

3.7.2 M^4RC

For the M^4RC experimental study, only the proposed supervisor scheme is tested. Three cases are tested in this study. The first two cases $M^4RC.1$ and $M^4RC.2$ are the same as those in the simulation studies in Section 3.6.2 which are shown in Table 3.4. The third case referred to as $M^4RC.3$ is similar to the $M^4RC.1$ case. However, in the $M^4RC.3$ case the loading is directly changed from Model 1 (full load) to Model 4 (unloaded), resulting in a larger percentage change of the parameters.

$M^4RC.1$ case

For the $M^4RC.1$ case, the controller is turned on at $t = 8.7$ seconds, and the loading condition is changed to Model 3 at $t = 27.3$ seconds. In order to observe the vibration amplitude for Model 3 without control, the controller is turned off

at $t = 63.8$ seconds. The controller is then turned on again at $t = 82.5$ seconds, before the loading condition is changed to Model 4 at $t = 100$ seconds. Again, the amplitude of Model 4 without control is observed by turning off the controller at $t = 137$ seconds. Finally the controller is turned back on at $t = 155$ seconds. The system response and the control signal are shown in Fig. 3.46. From the figure, it can be seen that if all the possible loading conditions are included in the model bank, the M⁴RC will give optimum attenuation for a system with varying loading condition. The supervisor scheme selects the corresponding controller associated with the current loading condition as shown in Fig. 3.47. The figure shows good agreement with the corresponding simulation result.

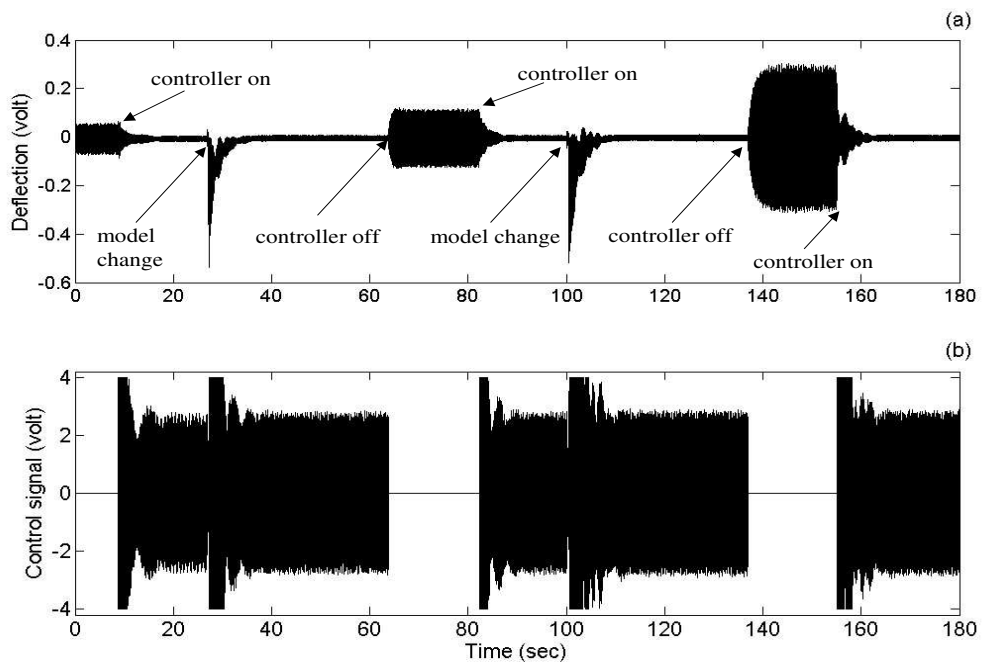


Figure 3.46: M⁴RC closed-loop response for the 1 \rightarrow 3 \rightarrow 4 model sequence.

M⁴RC.2 case

For the M⁴RC.2 case, the times at which the controller is turned on and off, and the loading condition changed are similar to the M⁴RC.1 case. The system

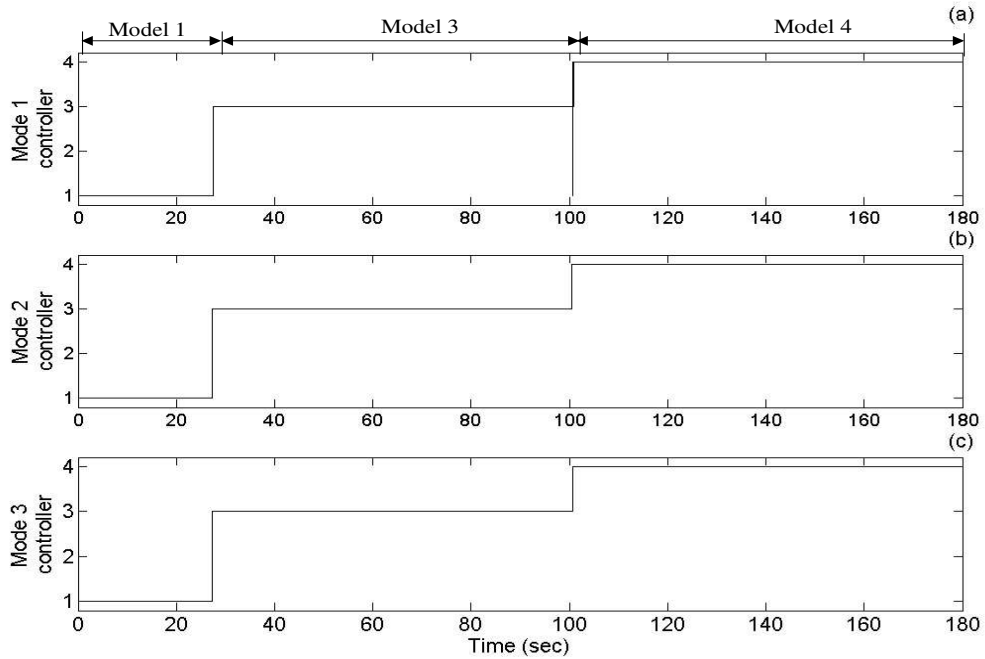


Figure 3.47: M^4RC switching behaviour for the $1 \rightarrow 3 \rightarrow 4$ model sequence.

response and control signal are shown in Fig. 3.48. The figure shows that the controller performs well for the Model 1 and Model 4 loading conditions. When the Model 2 loading condition, which is not included in the model bank, is applied, the supervisor selects the closest mode controller as shown by the switching behaviour given in Fig. 3.49. Since Controller 3 has the closest centre frequencies to those of Model 2 for all modes, as shown in Table 2.3, the supervisor then selects Controller 3 for all the modes. However, because Controller 3's centre frequency are significantly different from the natural frequencies of the current loading condition the attenuation performance could be poor, as can be seen for the Model 2 case. Overall, although there are times when the supervisor selects a less than ideal controller, the rapid switching that can degrade the performance of the system or lead to instability of the system does not occur in the proposed M^4RC .

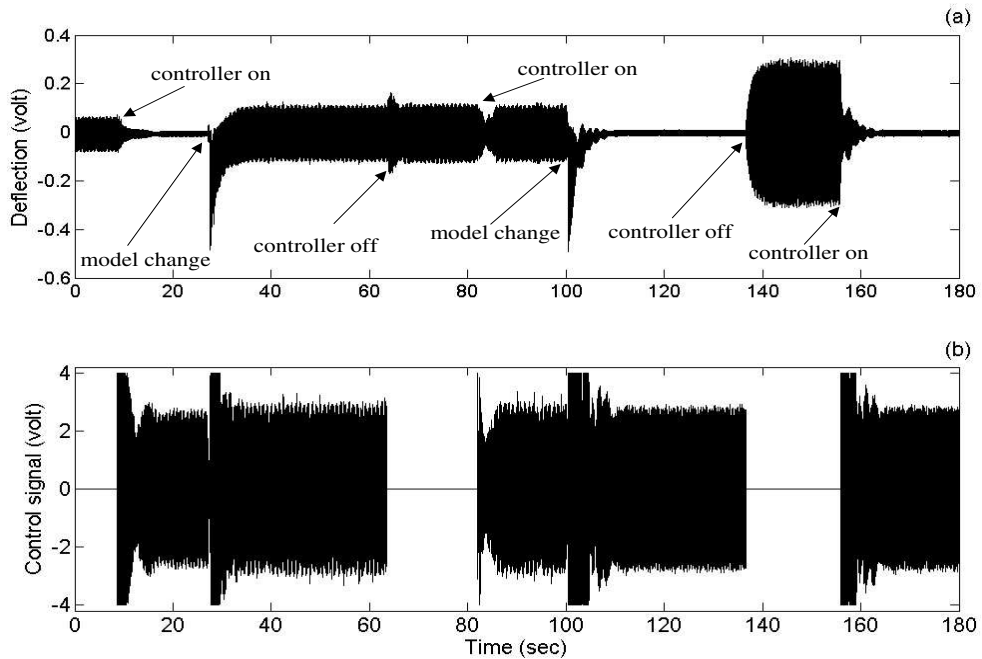


Figure 3.48: M^4RC closed-loop response for the $1 \rightarrow 2 \rightarrow 4$ model sequence.

$M^4RC.3$ case

For the $M^4RC.3$ case the controller is turned on at $t = 8.7$ seconds and the loading condition is changed to Model 4 at $t = 27.3$ seconds. To obtain a clear comparison between the amplitude of the vibration for Model 4 without and with control, the controller is turned off at $t = 63.8$ seconds and turned back on at $t = 82.5$ seconds. The system response and corresponding control signal, and the supervisor scheme switching behaviour are shown in Fig. 3.50 and Fig. 3.51, respectively. Fig. 3.50 shows that as long as all the possible loading conditions are included in the model bank, the M^4RC will give optimum attenuation, regardless of the magnitude of the parameter variations. By comparing Fig. 3.50 with Fig. 3.46 in the $M^4RC.1$ case, it can be seen that the only difference in the system response is the transition time when the loading condition is changed. The results show that larger load changes produce larger transition times.

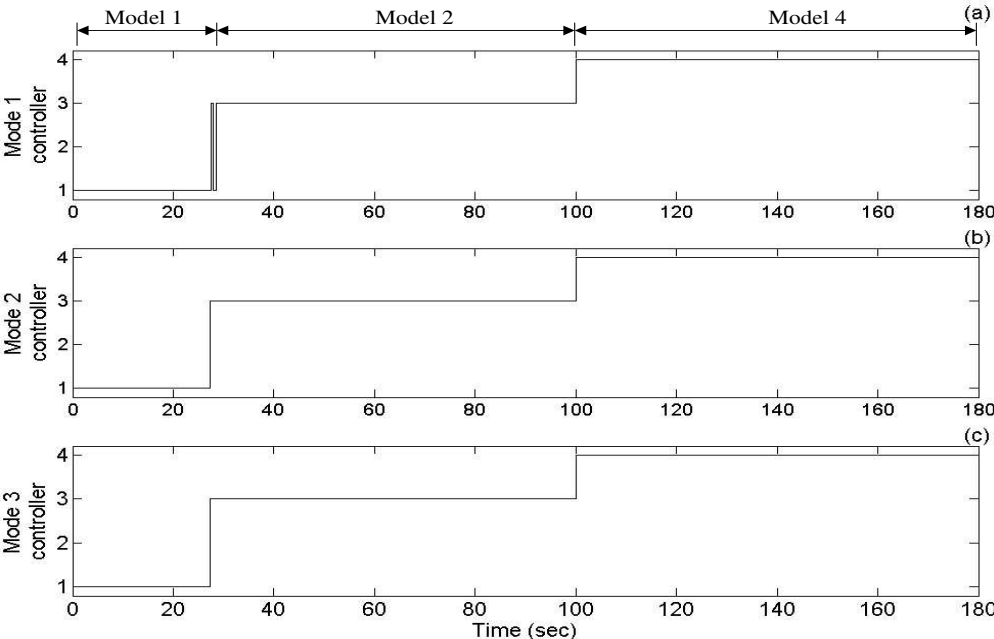


Figure 3.49: M^4RC switching behaviour for the $1 \rightarrow 2 \rightarrow 4$ model sequence.

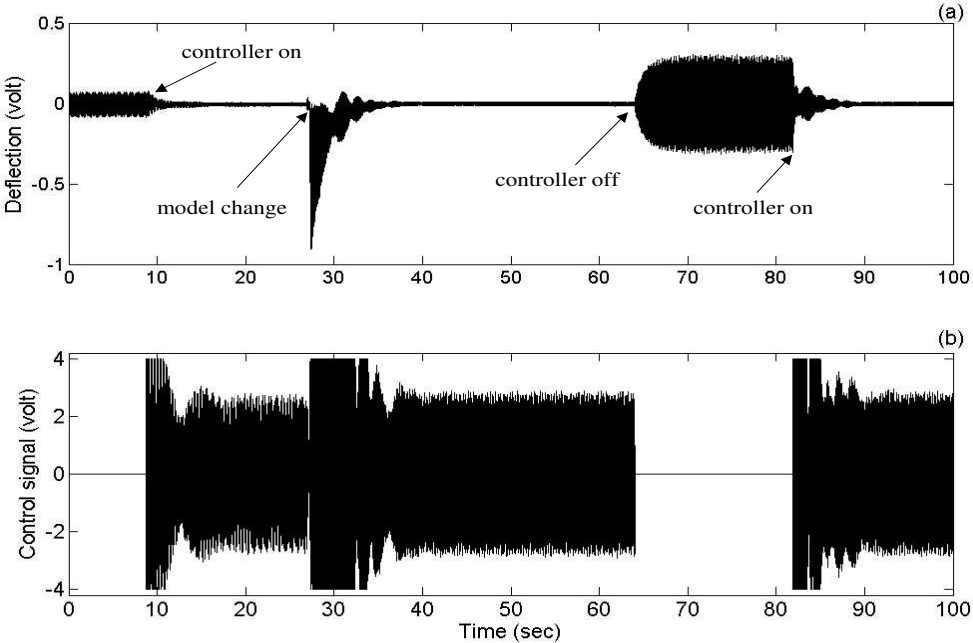


Figure 3.50: M^4RC closed-loop response for the $1 \rightarrow 4$ model sequence.

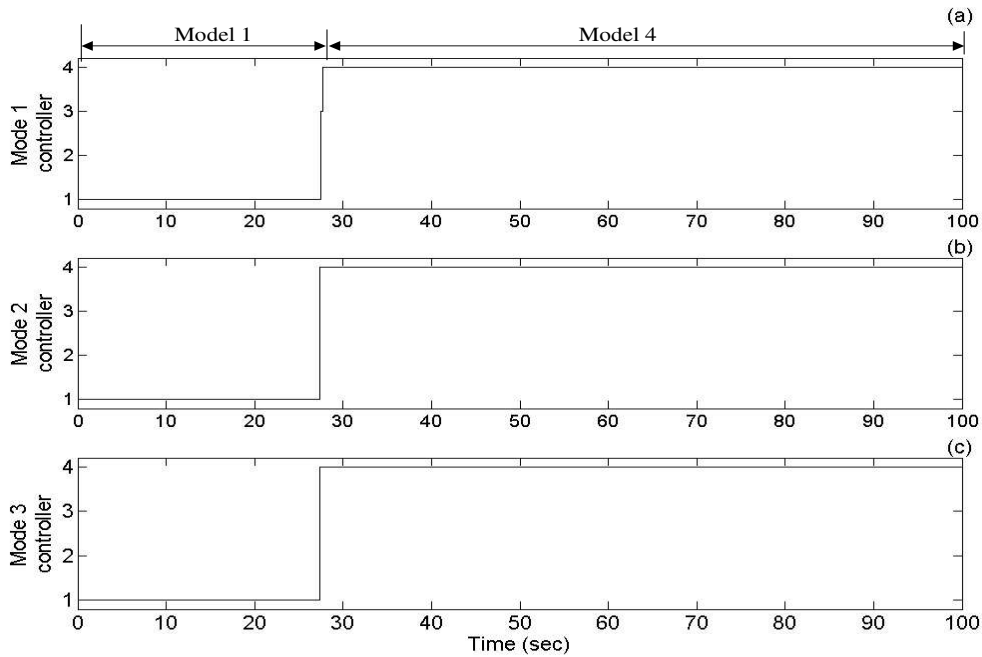


Figure 3.51: M^4RC switching behaviour for the $1 \rightarrow 4$ model sequence.

From the $M^4RC.2$ case, it can be seen that the controller fails to give optimum performance when the range of possible loading conditions is not fully represented in the model bank. The optimum performances of the M^4RC can be achieved by adding additional models to the model bank to cover all loading possibilities. However, this approach could be impractical especially for a large number of models. Therefore, it is important to find an alternative method for improving the performance of resonant control for systems with varying natural frequencies.

3.8 Summary

Due to its sensitivity to the variations of the natural frequencies of the system, the resonant control cannot give optimum performance when controlling the vibration of a flexible beam under varying load conditions. To improve the performance of the resonant control, the M^4RC with a reduced complexity supervisor scheme is

proposed in this chapter. The supervisor scheme design uses a filter bank scheme to determine how close the plant's vibration frequencies are to the natural frequencies of the *a priori* known models. At every sampling instant the supervisor identifies the closest model to the plant's current condition and selects the corresponding controller to produce the control signal. Because the basis for selection is only dependant on how close the models are to the plant's current conditions in the frequency domain, the supervisor scheme is computationally simple and is able to avoid rapid switching between controllers.

The simulation experimental studies are in agreement and show that the proposed M⁴RC gives good performance for the control of vibration in a cantilever beam with varying loads. However, when not all of the possible loading conditions are represented in the model bank, the performance of the controller is degraded. Although the performance can be improved by increasing the models in the model bank to represent all the possible loading conditions, the large number of models required make this method impractical. The large number of models necessitate the use of fast computers with lots of memory. Therefore, an alternative method such as adaptive control should be considered to obtain better performance for systems with unknown possible loading conditions.